Available online at www.sciencedirect.com
ScienceDirect
Physica D 237 (2008) 486–504
PHYSICA D
www.elsevier.com/locate/physd

Discrete breathers in nonlinear Schrödinger hypercubic lattices with arbitrary power nonlinearity

J. Dorignac*, J. Zhou, D.K. Campbell

College of Engineering, Boston University, 44 Cummington Street, Boston, MA 02215, United States

Received 15 September 2006; received in revised form 11 September 2007; accepted 18 September 2007
Available online 26 September 2007

Communicated by J. Lega

Abstract

We study two specific features of onsite breathers in Nonlinear Schrödinger systems on d-dimensional cubic lattices with arbitrary power nonlinearity (i.e., arbitrary nonlinear exponent, n): their wavefunctions and energies close to the anti-continuum limit – small hopping limit – and their excitation thresholds. Exact results are systematically compared to the predictions of the so-called *exponential ansatz* (EA) and to the solution of the *single nonlinear impurity model* (SNI), where all nonlinearities of the lattice but the central one, where the breather is located, have been removed. In 1D, the exponential ansatz is more accurate than the SNI solution close to the anti-continuum limit, while the opposite result holds in higher dimensions. The excitation thresholds predicted by the SNI solution are in excellent agreement with the exact results but cannot be obtained analytically except in 1D. An EA approach to the SNI problem provides an approximate analytical solution that is asymptotically exact as n tends to infinity. But the EA result degrades as the dimension, d, increases. This is in contrast to the exact SNI solution which improves as n and/or d increase. Finally, in our investigation of the SNI problem we also prove a conjecture by Bustamante and Molina [C.A. Bustamante, M.I. Molina, Phys. Rev. B 62 (23) (2000) 15287] that the limiting value of the bound state energy is universal when n tends to infinity.

Keywords: Discrete nonlinear Schrödinger equation; Anti-continuum limit; Exponential ansatz; Excitation thresholds; Lattice Green's functions; Nonlinear impurity

1. Introduction

The last decades have seen many efforts to understand nonlinear localization phenomena in various branches of physics (see for example Refs. [1–3] for some recent reviews). The cubic nonlinear Schrödinger equation (NLS) is a celebrated paradigm for continuous equations supporting solitons. Its ubiquity in physics arises from its generic occurrence in systems where small-amplitude wavepackets are to be described. Its discrete counterpart, the cubic Discrete Nonlinear Schrodinger Equation (DNLS) also plays an important role in modeling localization in lattices [4,5]. The DNLS was derived and studied by Holstein in his pioneering work on polarons in solids [6] and subsequently rederived in many other contexts such as biophysical systems [7], optical waveguide arrays [3,8], photonic crystals [9] and arrays of Bose–Einstein condensates [10,11] to name a few. For recent reviews on the subject the reader may consult Refs. [12,13] for example. Apart from the above-mentioned applications, the DNLS equation also arises in the context of Klein–Gordon lattices where it governs the slow modulations of small-amplitude modes [14–16].

A generalization of the DNLS equation to arbitrary power nonlinearities has also been investigated by many authors [17–23,25,26]. However, until recently the physical motivations for introducing such a generalization were somewhat elusive. For instance, it was proposed that a physical model with strong anharmonicity might require a nonlinearity higher than cubic or that a higher power nonlinearity could also be used to mimic the multi-dimensional behavior of the Schrödinger model [19]. But it seems fair to claim that the generalized DNLS equation was studied primarily as the discrete counterpart of the continuum generalized NLS equation, which is known to possess solitary wave solutions that can be stable or unstable, the latter possibly

* Corresponding author. Tel.: +1 617 358 1554; fax: +1 617 353 9393.
E-mail addresses: dorignac@bu.edu (J. Dorignac), jzhou@bu.edu (J. Zhou), dkcampbe@bu.edu (D.K. Campbell).

0167-2789/$ - see front matter © 2007 Elsevier B.V. All rights reserved.
doi:10.1016/j.physd.2007.09.018

blowing up in the critical or supercritical cases (see Refs. [17, 23] and references therein). More recently however, it has been shown in Ref. [27] that the generalized DNLS equation governs the slow modulations of small-amplitude *band-edge* modes in partially isochronous Klein–Gordon systems. The critical feature of these systems is that they possess onsite potentials (or a combination of the onsite and interaction potentials) that render their in-phase or anti-phase modes "partially harmonic" at low amplitude in the sense that, when expanded as power series in the energy density ε (energy per oscillator), their frequency reads $\omega \sim \omega_0 + \alpha\varepsilon^{\mu}$ where $\mu > 1$ is an integer. For generic potentials μ is typically equal to unity but for partially isochronous potentials μ can take on higher values.[1] It has been shown in Ref. [27] that the degree of the power nonlinearity in the DNLS equation governing the envelope of these modes is proportional to μ, whence a natural physical interpretation of the generalized DNLS equation.

Discreteness and the conservation of the norm of the wavefunction prevent any blow-up from taking place in DNLS. But another interesting phenomenon occurs: in the critical and supercritical cases, that is for $(n-1)d \geq 2$, the normalizable ground state, which following the convention we shall refer to as a *discrete breather* or also as a *bound state* throughout this paper, exists above a certain excitation threshold only (see for example [22–24]). Typically, if the hopping and the nonlinear strength are fixed, an excitation threshold will manifest itself as a minimal norm[2] for a breather solution to exist [20,22,23,25]. One of the purposes of the present study is to provide an approximate analytical expression for these excitation thresholds. We will derive this expression by means of an *exponential ansatz* that has been used in previous works on discrete breathers, polarons and bipolarons (see for example [20,28–30]). In 1D, the exponential ansatz turns out to be the exact solution to the *single nonlinear impurity model* (SNI) – a model where the nonlinearity has been removed from all but one lattice site [31–33]. The solutions to the SNI model and DNLS are close provided they are essentially localized on a single site of the lattice. This typically happens when the hopping term is small or when the nonlinear strength is large. If these two parameters are fixed, this also happens when the norm of the breather becomes large [23]. This is the limit where we expect the EA to provide the best results. Its exact accuracy needs to be checked, however, for we already know that it is not good enough to reproduce the bipolaron phase diagram of the 1D adiabatic Holstein–Hubbard model in the strong coupling limit [30]. Thus, in order to test its accuracy in the strongly localized limit, we will devote the first part of this study to a detailed comparison of the exponential ansatz results with the exact asymptotic ones and with the SNI solution. We will then use the same ansatz to locate the excitation thresholds and once again check how the results compare to the numerical and SNI solutions. Our analysis and results will hopefully make clear what physics one may expect the exponential ansatz to capture properly.

1.1. Nonlinear Schrödinger systems on lattices

In arbitrary dimension, d, we consider a nonlinear Schrödinger system on a hypercubic lattice with energy

$$F(\{\varphi\}) = \sum_{\boldsymbol{m}\in\mathbb{Z}^d} -\tau\varphi_{\boldsymbol{m}}^{*}\Delta\varphi_{\boldsymbol{m}} - \frac{1}{n}|\varphi_{\boldsymbol{m}}|^{2n}. \tag{1}$$

The nonlinearity n is an integer that satisfies $n \geq 2$. The wavefunction, $\varphi_{\boldsymbol{m}}$, where $\boldsymbol{m} \equiv (m_1, m_2, \ldots, m_d) \in \mathbb{Z}^d$, is normalized according to

$$\sum_{\boldsymbol{m}\in\mathbb{Z}^d} |\varphi_{\boldsymbol{m}}|^2 = 1. \tag{2}$$

The d-dimensional discrete Laplacian reads

$$\Delta\varphi_{\boldsymbol{m}} = \sum_{j=1}^{d} \varphi_{(m_1,\ldots,m_j+1,\ldots,m_d)} + \varphi_{(m_1,\ldots,m_j-1,\ldots,m_d)}. \tag{3}$$

Minimizing (1) with respect to $\varphi_{\boldsymbol{m}}$ under the normalization constraint yields a stationary generalized discrete nonlinear Schrödinger equation

$$-\tau\Delta\varphi_{\boldsymbol{m}} - |\varphi_{\boldsymbol{m}}|^{2(n-1)}\varphi_{\boldsymbol{m}} = E\varphi_{\boldsymbol{m}}, \tag{4}$$

where E, the Lagrange parameter associated with the normalization, is related to the energy F by

$$F(\{\varphi\}) = E + \frac{n-1}{n}\sum_{\boldsymbol{m}\in\mathbb{Z}^d} |\varphi_{\boldsymbol{m}}|^{2n}. \tag{5}$$

For simplicity, Eq. (4) will be called DNLS throughout this paper although this name is generally devoted to its non-stationary version obtained by replacing $E\varphi_{\boldsymbol{m}}$ by $i\dot{\varphi}_{\boldsymbol{m}}$ in the r.h.s. of Eq. (4).

1.2. Scaling

It proves sometimes convenient to work with a wavefunction $\psi_{\boldsymbol{m}}$ normalized to an arbitrary value, $\sum_{\boldsymbol{m}} |\psi_{\boldsymbol{m}}|^2 = \mathcal{N}$, and also to introduce a nonlinear strength, γ, that multiplies the nonlinear term in Eq. (4). In this case $\psi_{\boldsymbol{m}}$ obeys a seemingly more general DNLS equation than (4) that reads

$$-\hat{\tau}\Delta\psi_{\boldsymbol{m}} - \gamma|\psi_{\boldsymbol{m}}|^{2(n-1)}\psi_{\boldsymbol{m}} = \hat{E}\psi_{\boldsymbol{m}}, \tag{6}$$

with energy

$$\begin{aligned}\hat{F}(\{\psi\}) &= \sum_{\boldsymbol{m}\in\mathbb{Z}^d} -\hat{\tau}\psi_{\boldsymbol{m}}^{*}\Delta\psi_{\boldsymbol{m}} - \frac{\gamma}{n}|\psi_{\boldsymbol{m}}|^{2n} \\ &= \mathcal{N}\hat{E} + \gamma\frac{n-1}{n}\sum_{\boldsymbol{m}\in\mathbb{Z}^d} |\psi_{\boldsymbol{m}}|^{2n}.\end{aligned} \tag{7}$$

This equation will be used in the last section of this paper to analyze the existence of excitation thresholds in the creation of discrete breathers. Its advantage, both from the analytical

[1] For example, $V(x) = x^2/2 + \gamma x^3 + (5/2)\gamma^2 x^4$, is partially isochronous with $\mu = 2$ because $\omega = 1 + 210\gamma^4\varepsilon^2 + \mathcal{O}(\varepsilon^3)$.

[2] Depending on its sign, the breather energy may have a minimum or a maximum at the threshold.

and the numerical standpoint, is that it allows the study of the norm of discrete breathers as a function of their amplitude. The function $\mathcal{N}(\psi_0)$ turns out to be single-valued and in certain cases reaches a minimum, $\mathcal{N}^*$. Below this threshold value no breather exists.

The appearance of a norm threshold in Eq. (6) also manifests itself as a hopping threshold in Eq. (4). To see how, we introduce $\phi_{\boldsymbol{m}} = \psi_{\boldsymbol{m}}/\sqrt{\mathcal{N}}$ that is normalized to unity. Dividing Eq. (6) by $\gamma\mathcal{N}^{n-1}$ we find that $\phi_{\boldsymbol{m}}$ obeys Eq. (4) with

$$\tau = \frac{\hat{\tau}}{\gamma\mathcal{N}^{n-1}}. \tag{8}$$

This expression shows that the parameters $\hat{\tau}$, γ and $\mathcal{N}$ of Eq. (6) can be combined into a single one: namely, the effective hopping of the DNLS equation (4), valid for a nonlinear strength and a wavefunction normalized to unity. In particular, it shows how a threshold value for any of the three previously mentioned quantities translates into a threshold value for the effective hopping τ of Eq. (4). Moreover, we also see that the Lagrange parameters and energies of Eqs. (4) and (6) are related to each other according to

$$E = \frac{\hat{E}}{\gamma\mathcal{N}^{n-1}} \quad \text{and} \quad F(\{\phi\}) = \frac{\hat{F}(\{\psi\})}{\gamma\mathcal{N}^{n}}. \tag{9}$$

1.3. Organization of the paper

Throughout this article we will consider the solution to Eq. (4) (or Eq. (6)) to be located at the center of the lattice, $\boldsymbol{m} = \boldsymbol{0}$. In Section 2, we begin our investigation with a simple exponential ansatz (EA) solution to Eq. (4) close to the anti-continuum limit ($\tau = 0$). In Section 3, we compare it to the *exact* small τ perturbative solution and show that the results are the same up to order τ^{4n-2} in 1D while they agree up to order τ^2 in higher dimensions regardless of the nonlinear exponent n. This lack of improvement with n for $d \geq 2$, which arises because the EA is too symmetric, leads us to consider (in Section 4 another approximate solution to Eq. (4)): namely, the single nonlinear impurity (SNI) solution that is obtained by removing all nonlinearities from the hypercubic lattice but the one at the central site. After a brief introduction to the SNI problem, we evaluate its small τ limit and show that it agrees with the exact expansion up to order τ^{2n-2}. We then proceed by providing exact parametric expressions for the Lagrange parameter $\mathcal{E}$ and the energy $\mathcal{F}$ of the SNI solution as functions of τ. We use them to evaluate the hopping threshold $\tau^*_{n,d}$ beyond which no SNI breather exists, and we compare this result to a simple EA approach to the SNI problem. We show that the two solutions become asymptotically equivalent as the nonlinear exponent n tends to infinity. In addition, we prove a conjecture by Bustamante and Molina [33] regarding the universality of the limiting value of the Lagrange parameter[3] $\mathcal{E}$ as $n \to \infty$. In Section 5, we use Eq. (6) to analyze the existence of thresholds in the DNLS equation. We show that the exponential ansatz provides reliable parametric analytical expressions for all quantities (norm, Lagrange parameter, total energy,etc.) and allows for the determination of the threshold, if any, *provided the nonlinear exponent is large enough*. In this limit, the DNLS solution becomes sufficiently localized for the SNI approximation to hold. Given that in the same limit the EA solution to the SNI becomes more and more accurate, we use the results of Section 4 to derive simple expressions for all quantities at the threshold and assess their accuracy by evaluating their relative error with respect to numerical results. In Section 6, we summarize our results and present our conclusions.

2. Exponential ansatz

The d-dimensional normalized trial wavefunction for the exponential ansatz (EA) reads

$$\tilde{\varphi}_{\boldsymbol{m}} = \left(\frac{1-\lambda^2}{1+\lambda^2}\right)^{d/2} \lambda^{|\boldsymbol{m}|}, \tag{10}$$

where $|\boldsymbol{m}| = \sum_{i=1}^{d} |m_i|$ is the l_1-distance to the central peak located in $\boldsymbol{m} = \boldsymbol{0}$. Notice that the components of this EA wavefunction with the same distance $|\boldsymbol{m}|$ are equal. In this respect, the symmetry of this state is *higher* than the symmetry required for a solution to Eq. (4). Indeed, the exact solution to Eq. (4) that consists of a single peak at $\boldsymbol{m} = \boldsymbol{0}$ in the anti-continuum limit ($\tau = 0$) has to be invariant with respect to both an arbitrary permutation of its indices and a change of their sign as $\tau \neq 0$ since Eq. (4) satisfies these symmetries. Obviously, the EA wavefunction possesses these symmetries as well since they leave $|\boldsymbol{m}|$ invariant. However, as soon as the dimension is higher than one, other transformations can also leave the distance $|\boldsymbol{m}|$ invariant. For example, in $d = 2$, $\boldsymbol{m} = (2, 0)$ and $\boldsymbol{m}' = (1, 1)$ have the same distance, $|\boldsymbol{m}| = |\boldsymbol{m}'| = 2$, but are not related by a permutation or a sign inversion of their indices. Therefore, the EA wavefunction symmetry is higher than that strictly required as long as $d \geq 2$ and ansatz (10) is thus expected to provide better results in 1D than in higher dimension.

Inserting (10) into (1), we find the energy [28]

$$\tilde{F} = -\frac{1}{n}\left[\left(\frac{1-\lambda^2}{1+\lambda^2}\right)^n \frac{1+\lambda^{2n}}{1-\lambda^{2n}}\right]^d - \frac{4\tau d\lambda}{1+\lambda^2}, \ \lambda \in [0, 1]. \tag{11}$$

It is possible to verify that for $\tau \to 0$, the energy functional (11) has always a minimum for $\lambda_{n,d} = \tau + o(\tau^2)$. This is the ground state of (11). Higher order corrections to this formula are n- and d-dependent (see Appendix A).

Minimizing $\tilde{F}$ with respect to λ, we can expand the solution $\lambda_{n,d}(\tau)$ as a series in τ. Energies $\tilde{F}_{n,d}$ are then obtained by reinserting $\lambda_{n,d}(\tau)$ into (11) and expanding again. Proceeding thus, we have evaluated $\lambda_{n,d}(\tau)$ up to order τ^7 (see Appendix A) and find the corresponding energy accurate to order τ^8 to be given by

$$\tilde{F}_{n,d} = -\frac{1}{n} - 2d\tau^2 - \underbrace{2d\,(\xi - 2)\,\tau^4}_{n>2}$$

[3] $\mathcal{E}$ is referred to as bound state energy in Ref. [33].

$$-\underbrace{\frac{4d}{3}(5\xi^2-18\xi+16)\tau^6}_{n>3}$$
$$-\underbrace{\frac{2d}{3}(49\xi^3-252\xi^2+428\xi-240)\tau^8}_{n>4}+o(\tau^8), \quad (12)$$

where $\xi = nd$. In the above formula, the under-braces indicate the range of validity of the corresponding terms. The explicit formulae for $n = 2, 3, 4$ are given in Appendix B. The origin of such corrections is easily understood from (11) itself. In this expression, the term $[(1+\lambda^{2n})/(1-\lambda^{2n})]^d$ is responsible for corrections starting at order τ^{2n} in the energy (for, as said previously, $\lambda_{n,d} = \tau + o(\tau^2)$). Terms of order τ^{2k} in (12) are then generic for $k < n$ and are to be corrected as specified in Appendix B otherwise. These somewhat cumbersome but otherwise straightforward calculations are best carried out with a software able to perform algebraic manipulations. We have used Maple [38] to obtain our results. The corresponding programs are provided as supplementary material in the online version of this paper both in PDF format (sections C.1.1 and C.1.2, with a commented version of the programs) and as ready-to-use Maple codes, `ProgC11` and `ProgC12`.

From the physical perspective, neglecting $[(1+\lambda^{2n})/(1-\lambda^{2n})]^d$ in the energy expression (11) amounts to treating the problem of a *single nonlinear impurity*, $|\varphi_{\mathbf{0}}|^{2n}$, located at the center of the lattice (within the exponential ansatz approximation). This is clear from (1) and (10). Moreover, it is also clear that, in this limit, $\tilde{F}/d$ depends on the product nd only. This explains the exclusive ξ-dependence of the coefficients in (12), once divided by d. As we will see in the next section, this exclusive ξ-dependence is an artifact of the factorized form of the exponential ansatz that disappears once the appropriate symmetry of the wavefunction is taken into account. In Refs. [31,32], the *exact* solution to the *single nonlinear impurity* problem has been worked out by means of a self-consistent use of lattice Green's functions in 1D and 2D. We shall use this method in a forthcoming section to derive its small τ perturbative solution and compare it to the *exact* perturbative solution in any dimension and for arbitrary nonlinearities.

3. Small τ perturbative expansion

3.1. Wavefunction symmetry

In this section, we provide an *exact* perturbative solution to Eq. (4) such that $\varphi_{\boldsymbol{m}} = \delta_{\boldsymbol{m}\mathbf{0}}$ for $\tau = 0$ by expanding the wavefunction $\varphi_{\boldsymbol{m}}$ and the Lagrange parameter E as series in τ. We first use the symmetries previously mentioned in Section 2 to reduce the set of components to be calculated. Given that (4) is invariant with respect to an arbitrary permutation of the indices $(m_1, \ldots, m_d) \in \mathbb{Z}^d$ of $\boldsymbol{m}$ as well as an arbitrary change of their sign, we can restrict our investigation to components whose indices satisfy $m_1 \geq m_2 \geq \cdots \geq m_d \geq 0$. We shall denote the corresponding class by $\{\boldsymbol{m}\}$. For example, in $d = 5$, if $\boldsymbol{m} = (0, -1, 3, 1, 0)$ then it belongs to the class $\{\boldsymbol{m}\} = \{3, 1, 1\}$ (except for $\{\mathbf{0}\}$, we cut trailing zeros).

It is easy by inspection to establish the following properties of the perturbative series in τ for $\varphi_{\boldsymbol{m}}$ – henceforth the "τ-series": the τ-series for $\varphi_{\boldsymbol{m}}$ is odd (even) if $|\boldsymbol{m}|$ is odd (even) and its leading order is proportional to $\tau^{|\boldsymbol{m}|}$. According to the symmetry properties mentioned above, all components $\varphi_{\boldsymbol{m}}$ of the same class, $\{\boldsymbol{m}\}$, are equal and can be expanded as

$$\varphi_{\boldsymbol{m}} \equiv \varphi_{\{\boldsymbol{m}\}} = \tau^{|\boldsymbol{m}|} \sum_{j=0}^{\infty} \phi_{2j}^{\{\boldsymbol{m}\}}\, \tau^{2j}\,. \quad (13)$$

Inserting this expression in (1) and in (5), we see that both the energy and the Lagrange parameter are even in τ.

3.2. Energy up to order τ^8

To find the energy of the perturbative solution of (4) up to order τ^8, we need to expand the Lagrange parameter as

$$E = \sum_{j=0}^{4} E_{2j}\, \tau^{2j} + o(\tau^8) \quad (14)$$

and to evaluate the components $\varphi_{\boldsymbol{m}}$ with $|\boldsymbol{m}| \leq 4$. The complete list is $\mathcal{S} = \{\varphi_{\{0\}}, \varphi_{\{1\}}, \varphi_{\{2\}}, \varphi_{\{11\}}, \varphi_{\{3\}}, \varphi_{\{21\}}, \varphi_{\{111\}}, \varphi_{\{4\}}, \varphi_{\{31\}}, \varphi_{\{22\}}, \varphi_{\{211\}}, \varphi_{\{1111\}}\}$. To the same order the normalization of the wavefunction is obtained from

$$\begin{aligned}\mathcal{N}^2 = {} & |\varphi_{\{0\}}|^2 + 2d\left[|\varphi_{\{1\}}|^2 + |\varphi_{\{2\}}|^2 + |\varphi_{\{3\}}|^2 + |\varphi_{\{4\}}|^2\right] \\ & + 2A_d^2\left[|\varphi_{\{11\}}|^2 + |\varphi_{\{22\}}|^2\right] + 4A_d^2\left[|\varphi_{\{21\}}|^2 + |\varphi_{\{31\}}|^2\right] \\ & + \frac{4}{3}A_d^3|\varphi_{\{111\}}|^2 + 4A_d^3|\varphi_{\{211\}}|^2 \\ & + \frac{2}{3}A_d^4|\varphi_{\{1111\}}|^2 = 1 + o(\tau^8), \end{aligned} \quad (15)$$

where $A_d^k = d!/(d-k)!$ if $k \leq d$ and $A_d^k = 0$ else. The prefactors appearing in (15) are the number of elements of the corresponding class in dimension d. For instance, the number of elements in class $\{2\}$ is $2d$. The complete list is given by: $(\pm 2, 0, \ldots, 0), (0, \pm 2, \ldots, 0), \ldots, (0, 0, \ldots, \pm 2)$. Notice that the elements whose number of nonzero indices exceeds the dimension d are not involved and disappear from (15) because of the definition of A_d^k. Finally, because of (13), elements in class $\{\boldsymbol{m}\}$ need only be determined up to order $\tau^{8-|\boldsymbol{m}|}$ for (15) to hold. This means that the index j runs from 0 to $4 - |\boldsymbol{m}|$ in $\phi_{2j}^{\{\boldsymbol{m}\}}$. The number of coefficients $\phi_{2j}^{\{\boldsymbol{m}\}}$ to be evaluated is then $5 - |\boldsymbol{m}|$.

Inserting (13) and (14) in (4), we may write an equation for each of the components $\varphi_{\{\boldsymbol{m}\}} \in \mathcal{S}$. This is done in Appendix D. Solving the DNLS equation (4) (see also (D.1)) order-by-order in τ provides $5 - |\boldsymbol{m}|$ equations for each $\varphi_{\{\boldsymbol{m}\}}$ that allow for the determination of the $5 - |\boldsymbol{m}|$ coefficients $\phi_{2j}^{\{\boldsymbol{m}\}}$. The five remaining coefficients, E_{2j}, are determined from the five equations provided by the normalization condition (15). Once all the coefficients have been determined, we use Eq. (5) to obtain the energy $F_{n,d}$ as

$$F_{n,d} = -\frac{1}{n} - 2d\tau^2 - 2d\,(d-3+\xi)\,\tau^4$$

$$-\frac{4d}{3}\left(60-54d+10d^2+5\xi^2-27\xi+9d\xi\right)\tau^6$$
$$-\frac{2d}{3}\left(49\xi^3+227d^2\xi-1242d\xi+246d^3-3465\right.$$
$$\left.+\ 5031d-2052d^2+1443\xi+126d\xi^2-378\xi^2\right)\tau^8$$
$$+o(\tau^8) \tag{16}$$

where $\xi = nd$ and where the terms of order τ^{2k} are valid for $n > k$ only. For $2 \leq n \leq 4$, corrections to these generic coefficients are provided in Appendix B (formulae (B.4)–(B.6)). As in the case of the EA solution, these corrections originate from the *nonlinear impurities* lying in the immediate vicinity of the central one located at site $\mathbf{0}$. A way to obtain the result quoted above as well as those reported in Appendix B is to use the Maple program provided as supplementary material in the online version (Appendix C, section C.3, code `ProgC3`).

3.3. Energy accuracy and effective nonlinear part of the lattice

In what follows we discuss briefly the number and location of lattice nonlinearities needed to obtain a perturbative energy valid to an arbitrary order, τ^σ. From Eq. (13), it is clear that the leading order of $|\varphi_{\boldsymbol{m}}|^{2(n-1)}\varphi_{\boldsymbol{m}}$ is $\tau^{(2n-1)|\boldsymbol{m}|}$. Now, if we are to obtain a perturbative solution up to order τ^σ for the energy, we know from Eq. (D.1) that we must solve (4) up to order $\tau^{\sigma-|\boldsymbol{m}|}$ for $\varphi_{\boldsymbol{m}}$. This means that the nonlinear term $|\varphi_{\boldsymbol{m}}|^{2(n-1)}\varphi_{\boldsymbol{m}}$ plays a role in the equation if and only if

$$2n|\boldsymbol{m}| \leq \sigma. \tag{17}$$

In other words, for a given order σ and nonlinearity n, this condition determines the "effective" nonlinear part of the lattice that is, the distance $|\boldsymbol{m}|$ to the central site $\mathbf{0}$ up to which sites have to be considered nonlinear. This then yields the number and location of *nonlinear impurities* needed to derive the exact small τ expansion of the energy up to order τ^σ. The generic expression (16) corresponds to the result obtained for a single nonlinear impurity (located at site $\mathbf{0}$). According to condition (17), it is valid when the only solution to this inequality is $|\boldsymbol{m}| = 0$. This in turn implies that $2n > \sigma$, which explains the conditions displayed beneath each term of the series (16). *Thus, for a fixed nonlinearity n, the energies of the exact solution to* Eq. (4) *and to the single nonlinear impurity problem coincide up to order $\tau^{2(n-1)}$.* Notice that, contrary to the EA energy (12), once divided by d, the coefficients of the series (16) do not depend only on $\xi = nd$. This is a manifestation of the non-factorability of the true wavefunction solution to the single nonlinear impurity problem.

3.4. Exponential ansatz versus exact perturbative result

We now compare Eqs. (12) and (16). As we can see, for $d \geq 2$ they agree up to order τ^2 only. We can verify from the expressions given in Appendix B that this statement is also valid when $2 \leq n \leq 4$. This result is independent of the nonlinearity n and therefore, does not improve as n increases. The exponential ansatz is then not very accurate in the small τ regime in dimensions higher than unity. As previously explained, this essentially originates in its "excess" symmetry compared to the symmetry of the exact solution. In 1D, however, it is possible to see that Eqs. (12) and (16) coincide. In fact, it is easy to establish that in 1D, the exponential ansatz is an exact solution to the single impurity problem. This shows that its energy series is at least valid up to order $\tau^{2(n-1)}$. But in fact, a more careful analysis proves it to be valid up to order τ^{4n-2} and thus, to be as accurate as a *two nonlinear impurity* solution. This can be verified by comparing expressions (B.1) and (B.4) for $n = 2$ (and $d = 1$) that can be seen to agree up to order τ^6 rather than τ^2, as would be expected from a comparison with the single impurity solution (16). In some sense, when account is taken of the full nonlinearity of the problem within the exponential ansatz, the term $[(1+\lambda^{2n})/(1-\lambda^{2n})]$ correcting the single impurity term $[(1-\lambda^2)/(1+\lambda^2)]^n$ (see expression (11) and comments below) accurately captures the effect of the nonlinearity of sites 1 (and -1) but not the others. This is difficult to explain intuitively and only a careful analysis reveals it. Importantly, it is not true in higher dimensions. A numerical check of Eq. (16) for $n = 2$ and $d = 1, 2, 3$ and a comparison to the exponential ansatz solution (12) performed in Appendix G proves the correctness of these expressions.

3.5. Summary

In this section, we have derived the exact small τ perturbative expansion for the energy of the Discrete Nonlinear Schrödinger Equation on a hypercubic lattice with arbitrary dimension and compared it to results from the perturbative expansions of the exponential ansatz (EA) and the *single nonlinear impurity* (SNI) approaches. We shown that the SNI solution provides an expression for the energy that is accurate up to order $\tau^{2(n-1)}$ in the anti-continuum limit ($\tau \to 0$). Hence, the accuracy of this solution improves as the nonlinearity increases. We have argued that this improvement is due to the fact that the SNI wavefunction possesses the same symmetry as the exact one. In contrast, because of its "excessive" symmetry, the EA result is accurate only up to order τ^2 in dimension two and higher. But in 1D systems, the accuracy of the EA goes well beyond the SNI solution, as its energy coincides with the exact one up to order τ^{4n-2}. We have shown that the enhanced accuracy of the EA can be interpreted as resulting from the proper accounting of *two* nonlinear impurities located at sites 0 and 1 (and -1 by symmetry), and is hence obviously beyond the scope of the SNI approach. Nonetheless, the accuracy of the perturbative SNI solution strongly motivates a more detailed study of this approach, and we undertake this study in the ensuing section.

4. Single nonlinear impurity (SNI) problem

4.1. Brief review of the SNI problem

We now investigate the single nonlinear impurity problem and use the method proposed by [31,32] to derive its

exact solution in a hypercubic lattice of dimension d with nonlinearity n. The purposes of this section are two. First, to rederive the generic form of energy (16) from the exact results of the SNI problem. Second, to use the exact SNI results to study the existence of excitation thresholds for the creation of discrete breathers. Armed with these results, we shall see in the next section how these predictions of the EA and the SNI solutions compare with the numerical results regarding these excitation thresholds.

For the present purposes it is convenient to decompose the SNI Hamiltonian, H, into its *free particle* (tight binding) part, H_0, and its *nonlinear* part, H_1.

$$H = H_0 + H_1, \tag{18}$$

with (in an obvious notation)

$$H_0 = -\tau \sum_{n.n} |\boldsymbol{m}\rangle\langle\boldsymbol{n}|; \quad H_1 = \alpha|\boldsymbol{0}\rangle\langle\boldsymbol{0}|;$$
$$\alpha = -|\varphi_{\boldsymbol{0}}|^{2(n-1)}. \tag{19}$$

The kets $|\boldsymbol{m}\rangle$, $\boldsymbol{m} \in \mathbb{Z}^d$ form the lattice basis and any wavefunction $|\varphi\rangle$ can be expanded as $|\varphi\rangle = \sum_{\boldsymbol{m}\in\mathbb{Z}^d} \varphi_{\boldsymbol{m}}|\boldsymbol{m}\rangle$. The sum in H_0 extends to nearest neighbors. By convention the Schrödinger equation associated with Hamiltonian (18) is $H|\varphi\rangle = \mathcal{E}|\varphi\rangle$. It reads

$$-\tau\,\Delta\varphi_{\boldsymbol{m}} - |\varphi_{\boldsymbol{0}}|^{2(n-1)}\,\varphi_{\boldsymbol{0}}\,\delta_{\boldsymbol{m},\boldsymbol{0}} = \mathcal{E}\varphi_{\boldsymbol{m}}. \tag{20}$$

The corresponding energy functional is given by

$$\mathcal{F} = -\tau \sum_{\boldsymbol{m}\in\mathbb{Z}^d} \varphi^*_{\boldsymbol{m}}\Delta\varphi_{\boldsymbol{m}} - \frac{1}{n}|\varphi_{\boldsymbol{0}}|^{2n}. \tag{21}$$

Notice that $\mathcal{F} \neq \langle\varphi|H|\varphi\rangle = \mathcal{E}$ which is due to the fact that H_1 depends on $\varphi_{\boldsymbol{0}}$ (and is thus nonlinear). The Lagrange parameter $\mathcal{E}$ – bound state energy – is related to the total energy $\mathcal{F}$ by

$$\mathcal{F} = \mathcal{E} + \frac{n-1}{n}|\varphi_{\boldsymbol{0}}|^{2n}. \tag{22}$$

It is clear that this expression is the same as Eq. (5) except for the second term that retains the central nonlinearity only. The resolvents (Green's functions) associated with H and H_0 are respectively given by

$$G(z) = (z - H)^{-1} \quad \text{and} \quad G^{(0)}(z) = (z - H_0)^{-1}, z \in \mathbb{C}. \tag{23}$$

Defining their lattice components as $G_{\boldsymbol{mn}}(z) = \langle\boldsymbol{m}|G(z)|\boldsymbol{n}\rangle$ and the corresponding expression for $G^{(0)}_{\boldsymbol{mn}}(z)$, we obtain[4]

$$G_{\boldsymbol{mn}}(z) = G^{(0)}_{\boldsymbol{mn}}(z) + \frac{\alpha G^{(0)}_{\boldsymbol{m0}}(z)G^{(0)}_{\boldsymbol{0n}}(z)}{1 - \alpha G^{(0)}_{\boldsymbol{00}}(z)}. \tag{24}$$

According to the general properties of lattice Green's functions [35], the pole of $G(z)$ provides the bound state energy $z = \mathcal{E}$ and the residue of $G_{\boldsymbol{mn}}(z)$ at $z = \mathcal{E}$, the density matrix element $\rho_{\boldsymbol{mn}} = \varphi^*_{\boldsymbol{m}}\varphi_{\boldsymbol{n}}$. Thus, from (24), the bound state energy is related to the value of its wavefunction at the center of the lattice by $G^{(0)}_{\boldsymbol{00}}(\mathcal{E}) = \alpha^{-1} = -|\varphi_{\boldsymbol{0}}|^{-2(n-1)}$ while $|\varphi_{\boldsymbol{0}}|^2 = \rho_{\boldsymbol{00}}$ is given by

$$|\varphi_{\boldsymbol{0}}|^2 = \operatorname{Res} G_{\boldsymbol{00}}(z)|_{z=\mathcal{E}} = -\frac{[G^{(0)}_{\boldsymbol{00}}(\mathcal{E})]^2}{G^{(0)'}_{\boldsymbol{00}}(\mathcal{E})}, \tag{25}$$

where the prime denotes a derivative with respect to z. Combining these results, we finally obtain an *exact* equation that allows for the determination of the bound state energy $\mathcal{E}$,

$$\frac{[G^{(0)}_{\boldsymbol{00}}(\mathcal{E})]^{2n-1}}{[-G^{(0)'}_{\boldsymbol{00}}(\mathcal{E})]^{n-1}} = -1. \tag{26}$$

This equation is valid in arbitrary dimension d and for any nonlinearity n. To proceed further, we need an explicit expression for the free particle Green's function $G^{(0)}_{\boldsymbol{00}}(z)$ in a d-dimensional hypercubic lattice. It is given by (see for example [35,36])

$$G^{(0)}_{\boldsymbol{00}}(z) = \frac{1}{(2\pi)^d}\int_{-\pi}^{\pi} \frac{\mathrm{d}^d k}{z + 2\tau\sum_{l=1}^{d}\cos k_l} = -\frac{1}{2\tau}\mathcal{L}_d\left(-\frac{z}{2\tau}\right),$$
$$\Re z < -2\tau d. \tag{27}$$

The function $\mathcal{L}_d(s)$ is the Laplace transform of the dth power of the modified Bessel function I_0,

$$\mathcal{L}_d(s) = \int_0^\infty \mathrm{e}^{-su}\,[I_0(u)]^d\,\mathrm{d}u. \tag{28}$$

The last equality in (27) has been obtained from[5] $-\nu^{-1} = \int_0^\infty \mathrm{e}^{\nu x}\mathrm{d}x$ for $\Re\nu < 0$ and the integral representation of the modified Bessel function $I_0(z) = \frac{1}{\pi}\int_0^\pi \mathrm{e}^{z\cos\theta}\mathrm{d}\theta$ [37]. For the lowest values of d, $\mathcal{L}_d(s)$ can be evaluated exactly in terms of elementary ($d = 1$) or special ($d = 2, 3, 4$) functions of increasing complexity (see for instance [39–42][6] and references therein). In the general case, expanding $I_0^d(u)$ as a power series in u and integrating term-by-term yields

$$\mathcal{L}_d(s) = \frac{1}{s}\sum_{\sigma=0}^{\infty}\frac{(2\sigma)!}{2^{2\sigma}}\frac{D^{(d)}_\sigma}{s^{2\sigma}}, \quad \text{where}$$
$$D^{(d)}_\sigma = \sum_{\substack{k_1+\cdots+k_d=\sigma\\ k_i\geq 0}} \frac{1}{[k_1!k_2!\cdots k_d!]^2}. \tag{29}$$

In particular, $D^{(1)}_\sigma = \frac{1}{(\sigma!)^2}$, $D^{(2)}_\sigma = \frac{(2\sigma)!}{(\sigma!)^4}$, $D^{(3)}_\sigma = {}_3F_2(\frac{1}{2}, -\sigma, -\sigma; 1, 1; 4)/(\sigma!)^2$, where ${}_3F_2(a, b, c; d, e; z)$ de-

[4] Using (23) and dropping the z-dependence of the Green's functions for convenience, we have $(z - H_0 - H_1)G = 1$ that is, $(1 - G^{(0)}H_1)G = G^{(0)}$. Using (19) and bracketing this equality with $\langle\boldsymbol{m}|$ and $|\boldsymbol{n}\rangle$ yields $G_{\boldsymbol{mn}} - \alpha G^{(0)}_{\boldsymbol{m0}}G_{\boldsymbol{0n}} = G^{(0)}_{\boldsymbol{mn}}$. Specializing to $\boldsymbol{m} = 0$, we find $G_{\boldsymbol{0n}} = G^{(0)}_{\boldsymbol{0n}}/(1 - \alpha G^{(0)}_{\boldsymbol{00}})$, whence the result (24).

[5] The reason for choosing $\Re z < -2\tau d$ in (27) is because this formula is to be used at $z = \mathcal{E}$. The bound state energy $\mathcal{E}$ lies below the band-edge of the continuum $2\tau\sum_{l=1}^{d}\cos k_l$, hence $\mathcal{E} < -2\tau d$.

[6] These papers do not give the Laplace transform $\mathcal{L}_d(s)$ defined in (33) directly. But they evaluate the function

$$P_d(z) = \frac{1}{\pi^d}\int_0^\pi \frac{\mathrm{d}^d k}{1 - \frac{z}{d}\sum_{i=1}^{d}\cos k_i} = \frac{d}{z}\mathcal{L}_d\left(\frac{d}{z}\right). \text{ Hence } \mathcal{L}_d(s) = \frac{1}{s}P_d\left(\frac{d}{s}\right).$$

notes the generalized hypergeometric function. For an arbitrary dimension d, we can evaluate the first coefficients: $D_0^{(d)} = 1$, $D_1^{(d)} = d$, $D_2^{(d)} = d(2d-1)/4$, $D_3^{(d)} = d(6d^2 - 9d + 4)/36$, etc.

4.2. Energy in the anti-continuum limit ($\tau \to 0$)

To compare with our perturbative results, we need to solve Eq. (26) for the bound state energy $\mathcal{E}$ in the anti-continuum limit, $\tau \to 0$. We first expand $\mathcal{E}$ as a series in τ. Noticing that a change of variable $k_l \to k_l + \pi$ simply changes the sign of τ in (27), we see that $G_{\mathbf{00}}^{(0)}(z)$ is even in τ and then, so does $\mathcal{E}$. Moreover, as $\varphi_{\mathbf{0}} \to 1$ when $\tau \to 0$, the leading order of $\mathcal{E}$ is -1 in this limit. Then,

$$\mathcal{E} = -1 + \sum_{j=1}^{\infty} \mathcal{E}_{2j}\, \tau^{2j}. \tag{30}$$

Now we expand $-2\tau/\mathcal{E}$ as a power series in τ and use (27) and (29) to obtain a τ-series for $G_{\mathbf{00}}^{(0)}(\mathcal{E})$ and $G_{\mathbf{00}}^{(0)'}(\mathcal{E})$ whose coefficients are functions of the parameters $\mathcal{E}_{2j}$. Inserting these results in (26) and solving order-by-order in τ yields eventually the parameters $\mathcal{E}_{2j}$: $\mathcal{E}_2 = 2\xi - 4d$, $\mathcal{E}_4 = 6\xi^2 - (18+2d)\xi - 8d^2 + 24d$, etc., where $\xi = nd$. Once $\mathcal{E}$ is known to some order in τ, it can be used to calculate $|\varphi_0|^2$ to the same accuracy, thanks to (25). The result is finally reinserted into (22) to obtain the total energy

$$\begin{aligned}\mathcal{F}_{n,d} = &-\frac{1}{n} - 2d\tau^2 - 2d(d-3+\xi)\tau^4 \\ &- \frac{4d}{3}(60 - 54d + 10d^2 + 5\xi^2 - 27\xi + 9d\xi)\tau^6 \\ &- \frac{2d}{3}(49\xi^3 + 227d^2\xi - 1242d\xi + 246d^3 \\ &- 3465 + 5031d - 2052d^2 + 1443\xi \\ &+ 126d\xi^2 - 378\xi^2)\tau^8 + o(\tau^8).\end{aligned} \tag{31}$$

This result is of course the same as the energy derived in (16), except for the restrictions upon the coefficients that have disappeared since no nonlinear impurity but the central one is present in this SNI model. This result is then valid for any n and d. Although tedious, the calculations needed to produce this expression are straightforward and automatic once implemented in the Maple code named `ProgC2` provided as supplementary material in the online version of this paper in Appendix C, section C.2.

4.3. Hopping threshold for the existence of breathers in the SNI problem

For values of the hopping parameter τ that are not small, Eq. (26) allows for the derivation of the exact energy of the bound state(s), if any. For that purpose, it is convenient to introduce a parameter that measures the "distance" between the energies of the bound state and the continuum band-edge (with respect to the middle of the continuum band), $\kappa = -2\tau d/\mathcal{E}$. As $\mathcal{E} < -2\tau d$, this parameter takes on values within the range $[0, 1)$. The limit $\kappa \to 0$ corresponds to $\tau \to 0$ that is, to the anti-continuum limit (as we have seen previously, $\mathcal{E} \to -1$ in this limit). On the other hand, it is obvious that $\kappa \to 1$ as $\mathcal{E}$ comes close to the continuum band-edge energy $-2\tau d$. Written in terms of κ, Eq. (26) can be cast into the form

$$g_{n,d}(\kappa) = \tau, \quad \kappa = \frac{-2\tau d}{\mathcal{E}} \in [0, 1), \tag{32}$$

with

$$g_{n,d}(\kappa) = \frac{1}{2}\frac{[\mathcal{L}_d(s)]^{2n-1}}{[-\mathcal{L}_d'(s)]^{n-1}}|_{s=d/\kappa}\,, \tag{33}$$

where the prime denotes a derivative with respect to s. Using Eqs. (33) and (22) we can now provide a parametric representation for τ, $\mathcal{E}$ and $\mathcal{F}$ in terms of κ,

$$\begin{aligned}&\tau = g_{n,d}(\kappa); \quad \mathcal{E} = -\frac{2d}{\kappa} g_{n,d}(\kappa); \\ &\mathcal{F}_{n,d} = -2g_{n,d}(\kappa)\left[\frac{d}{\kappa} + \frac{n-1}{n}\frac{\mathcal{L}_d\left(\frac{d}{\kappa}\right)}{\mathcal{L}_d'\left(\frac{d}{\kappa}\right)}\right].\end{aligned} \tag{34}$$

The last equation has been obtained thanks to Eq. (25) where the Green's function has been expressed in terms of $\mathcal{L}_d(s)$. This representation provides an implicit analytical expression for $\mathcal{E}(\tau)$ and $\mathcal{F}_{n,d}(\tau)$.

4.3.1. 1D lattice, $d = 1$

The 1D case is very special as it can be solved exactly by means of the exponential ansatz (10). Indeed, inserting the EA form of the wavefunction into the SNI equation (20) yields immediately a parametric solution given in terms of the localization parameter $\lambda \in [0, 1]$

$$\begin{aligned}&\tau = \frac{\lambda}{1-\lambda^2}\left[\frac{1-\lambda^2}{1+\lambda^2}\right]^{n-1}; \quad \mathcal{E} = -\left[\frac{1-\lambda^2}{1+\lambda^2}\right]^{n-2}; \\ &\mathcal{F}_{n,1} = \mathcal{E} + \frac{n-1}{n}\left[\frac{1-\lambda^2}{1+\lambda^2}\right]^{n}.\end{aligned} \tag{35}$$

Using these expressions, we can provide a relation between the parameter $\kappa = -2\tau/\mathcal{E}$, measuring the "distance" of the bound state energy to the continuum band-edge, and the localization parameter λ. It takes the remarkably simple form

$$\kappa = \frac{2\lambda}{1+\lambda^2}. \tag{36}$$

Let us now obtain the SNI solution by using the Green's function approach. Using Eqs. (32) and (33) and $\mathcal{L}_1(s) = (s^2-1)^{-1/2}$ [39], we find

$$g_{n,1}(\kappa) = \frac{\kappa}{2}\left(1-\kappa^2\right)^{\frac{n}{2}-1}, \tag{37}$$

and, upon using Eqs. (34), this eventually yields

$$\begin{aligned}&\tau = \frac{\kappa}{2}\left[1-\kappa^2\right]^{\frac{n}{2}-1}; \quad \mathcal{E} = -\left[1-\kappa^2\right]^{\frac{n}{2}-1}; \\ &\mathcal{F}_{n,1} = -\frac{1}{n}\left[1-\kappa^2\right]^{\frac{n}{2}-1}[1 + (n-1)\kappa^2].\end{aligned} \tag{38}$$

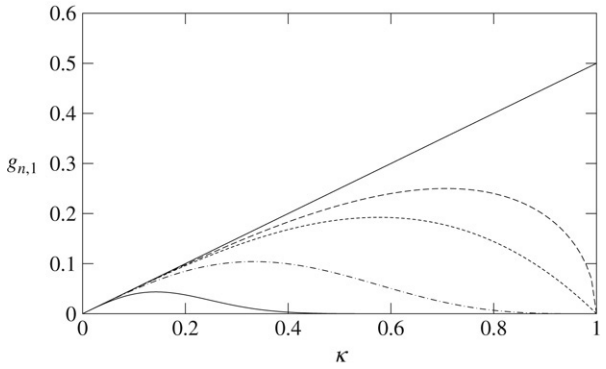

Fig. 1. Functions $g_{n,1}(\kappa)$ for $n = 2, 3, 4, 10, 50$. As n increases, the maximum of $g_{n,1}(\kappa)$ shifts towards $\kappa = 0$.

We can verify by using Eq. (36) that these equations are equivalent to (35). The two methods are then merely reparametrizations of one another in terms of distance to the continuum or localization length. The curves $g_{n,1}(\kappa)$ corresponding to different values of the nonlinearity n have been drawn in Fig. 1. As we can see, they all posses a maximum for $\kappa \in [0, 1]$. This indicates that above a certain n-dependent critical hopping value, $\tau^*_{n,1}$, no bound state exists anymore. An essential difference occurs between the particular case $n = 2$ and higher values of n. For $n = 2$, $g_{2,1} = \kappa/2$ and Eq. (32) indicates that a single bound state exists for all values of $\tau < \tau^*_{2,1} = 1/2$. Strangely, its Lagrange parameter does not depend on τ and is given by $\mathcal{E} = -1$. But its energy, $\mathcal{F}_{2,1} = -1/2 - 2\tau^2$, does depend on τ.

For $n > 2$, the number of bound states below $\tau^*_{n,1}$ is two. The closest to $\kappa = 0$ can be shown to be stable while the other one is unstable [20]. Actually, we see this stability difference on the graph of the functional $\mathcal{F}$ (see Fig. 2, left panel). The bound state the closest to $\lambda = 0$ – that is also the closest to $\kappa = 0$ given Eq. (36) – corresponds to a minimum of $\mathcal{F}$ while the other one corresponds to a maximum of the functional. On Fig. 3 (left panel), these bound states are the intersections of the curve $g_{n,1}(\kappa)$ with the horizontal line representing the value of τ. For $\tau \to 0$, the stable bound state is the one whose energy has been evaluated perturbatively in expression (31). The other one (for $n > 2$) comes close to the continuum band in this limit and disappears by merging with it as $\kappa = 1$. In this limit, its localization length, $|\ln\lambda|^{-1}$, becomes infinite, while the localization length of the stable bound state tends to zero.

One of the great advantages of the parametric form (38) (or (35)), is to provide at once the energies $\mathcal{F}_{n,1}$ of both the *stable* and *unstable* bound states with respect to τ. These energies have been plotted in Fig. 4 for various nonlinearities. The lower branch of $\mathcal{F}_{n,1}(\tau)$ gives the energy of the stable bound state while the upper one corresponds to the energy of the unstable bound state. The turning point corresponds to the critical hopping value, $\tau^*_{n,1}$, beyond which no bound state exists. It is easy to evaluate all quantities at criticality by finding the maximum of $g_{n,1}(\kappa)$. We obtain

$$\kappa^*_{n,1} = \frac{1}{\sqrt{n-1}}; \quad \lambda^*_{n,1} = \sqrt{n-1} - \sqrt{n-2}, \tag{39}$$

and

$$\tau^*_{n,1} = \frac{1}{2\sqrt{n-1}}\left[\frac{n-2}{n-1}\right]^{\frac{n}{2}-1}; \qquad \mathcal{E}^*_{n,1} = -\left[\frac{n-2}{n-1}\right]^{\frac{n}{2}-1};$$
$$\mathcal{F}^*_{n,1} = -\frac{2}{n}\left[\frac{n-2}{n-1}\right]^{\frac{n}{2}-1}. \tag{40}$$

For $n = 2$ these expressions are still valid provided they are evaluated as limits ($n \to 2$). For $n \to \infty$, their asymptotic behaviors read

$$\kappa^*_{n,1} \sim \frac{1}{\sqrt{n}}; \quad \lambda^*_{n,1} \sim \frac{1}{2\sqrt{n}}; \quad \tau^*_{n,1} \sim \frac{\mathrm{e}^{-1/2}}{2\sqrt{n}};$$
$$\mathcal{E}^*_{n,1} \sim -\mathrm{e}^{-1/2}; \quad \mathcal{F}^*_{n,1} \sim -\frac{2}{n}\mathrm{e}^{-1/2}. \tag{41}$$

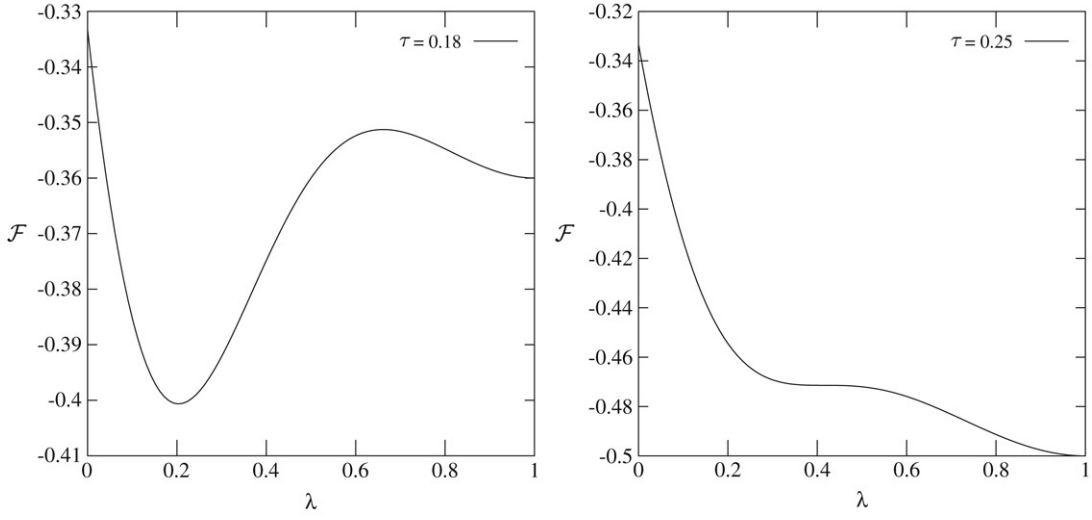

Fig. 2. SNI energy functional $\mathcal{F}$ in 1D for $n = 3$ versus the localization parameter λ. Left panel, $\tau = 0.18 < \tau^*_{3,1}$. The minimum around $\lambda \simeq 0.2$ represents the stable bound state solution. The maximum around $\lambda \simeq 0.65$ represents the unstable bound state. Right panel, $\tau = \tau^*_{3,1} = 1/4$. For this critical value of τ, the minimum and the maximum merges at $\lambda^*_{3,1} = \sqrt{2} - 1$. For $\tau > \tau^*_{3,1}$ no bound state exists.

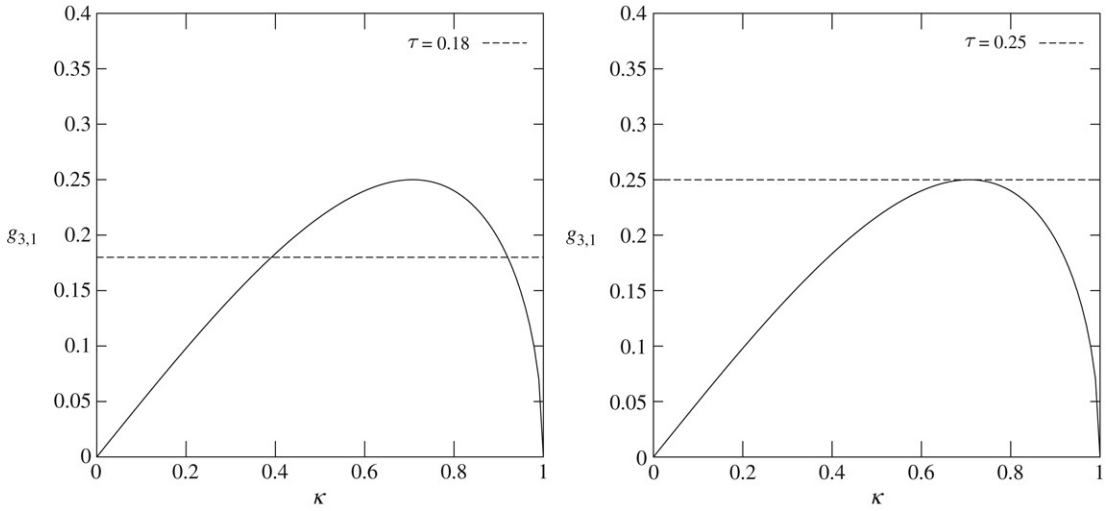

Fig. 3. Graphic solution to Eq. (32), $g_{3,1}(\kappa) = \tau$, for $\tau = 0.18 < \tau^*_{3,1}$ (left panel) and for $\tau = \tau^*_{3,1} = 1/4$ (right panel). On the left panel, the stable bound state corresponds to the intersection near $\kappa = 0.4$ while the other intersection around $\kappa = 0.9$ corresponds to the unstable bound state. On the right panel, the two bound states have merged at $\kappa^*_{3,1} = 1/\sqrt{2}$.

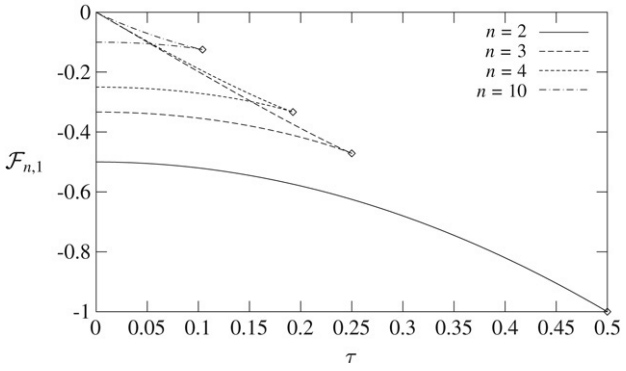

Fig. 4. Energies $\mathcal{F}_{n,1}(\tau)$ of the stable (lower branch) and unstable (upper branch for $n > 2$) bound states for various nonlinearities. Diamond symbols mark the turning points $(\tau^*_{n,1}, \mathcal{F}^*_{n,1})$ as given by Eqs. (40).

4.3.2. Higher dimensions

For $d \geq 1$, the SNI problem cannot be solved exactly with the exponential ansatz. But whenever an analytical expression is available for the Laplace transform $\mathcal{L}_d(s)$, Eqs. (34) provide exact parametric expressions for the Lagrange parameter $\mathcal{E}_{n,d}$ and the energy $\mathcal{F}_{n,d}$ versus the hopping τ. This is the case in $d = 2, 3, 4$. These expressions are given here for $d = 2$ and the reader is referred to Refs. [40–42] for explicit analytical results in 3D and 4D. Using $\mathcal{L}_2(s) = \frac{2}{\pi s} K(\frac{2}{s})$ [39], where $K(k) = \int_0^{\pi/2} [1 - k^2 \sin^2\theta]^{-1/2} \mathrm{d}\theta$ is the complete elliptic integral of the first kind, we obtain

$$g_{n,2}(\kappa) = \frac{2^n}{4\pi^n} \kappa (1-\kappa^2)^{n-1} \frac{K(\kappa)^{2n-1}}{E(\kappa)^{n-1}}, \tag{42}$$

where $E(k) = \int_0^{\pi/2} [1 - k^2 \sin^2\theta]^{1/2} \mathrm{d}\theta$ is the complete elliptic integral of the second kind. The same expression, although with different notations,[7] has been obtained in [32]. Some curves $g_{n,2}(\kappa)$ have been drawn in Fig. 5 (left panel). In contrast to the 1D case, the number of bound states is always two below the hopping critical value $\tau^*_{n,2}$ and zero above, even for $n = 2$. The parametric equations (34) have the particular form

$$\begin{aligned} &\tau = g_{n,2}(\kappa); \quad \mathcal{E} = -\frac{4}{\kappa} g_{n,2}(\kappa); \\ &\mathcal{F}_{n,2} = -\frac{4 g_{n,2}(\kappa)}{\kappa} \left[1 - \frac{n-1}{n} (1-\kappa^2) \frac{K(\kappa)}{E(\kappa)} \right]. \end{aligned} \tag{43}$$

For $n = 2$ to $n = 5$, energies $\mathcal{F}_{n,2}$ have been drawn in Fig. 5 (right panel) together with their exponential ansatz approximations, $\tilde{\mathcal{F}}_{n,2}$ (see Section 4.3.4). As we can see, in contrast to the 1D case, the lowest curve (for $n = 2$) now has two branches corresponding to a stable (lower branch) and an unstable (upper branch) bound states.

In 3D, we have used the analytical expression provided in [41] to calculate the curves $g_{n,3}(\kappa)$. These are represented in Fig. 6 (left panel) for various values of n and compared to their EA counterparts (see next section). Energies $\mathcal{F}_{n,3}(\tau)$ are displayed in the right panel of the same figure. As we can see, the major difference between the exact $g_{n,3}(\kappa)$ curves and their EA counterparts is that exact curves tend to zero as the Lagrange parameter reaches the continuum band-edge ($\kappa \to 1$) while the EA counterparts do not. Actually, an asymptotic analysis of the behavior of the Laplace transform $\mathcal{L}_d(s)$ and its derivative indicates that the opening of a gap at $\kappa = 1$ for $g_{n,d}(\kappa)$ only occurs in $d = 1$ for $n = 2$ or when $d \geq 5$. This fact is important because a gap at $\kappa = 1$ implies that a *single bound state* exists for $0 \leq \tau < g_{n,d}(1)$ while for $g_{n,d}(1) \leq \tau < \tau^*_{n,d}$ *two bound states* exist that disappear when $\tau > \tau^*_{n,d}$.

[7] In 2D, the nonlinear parameter γ of Ref. [32] is related to our hopping parameter via $\gamma \equiv 1/(4\tau)$ and the quantity $m = 1/z^2$ corresponds to κ^2.

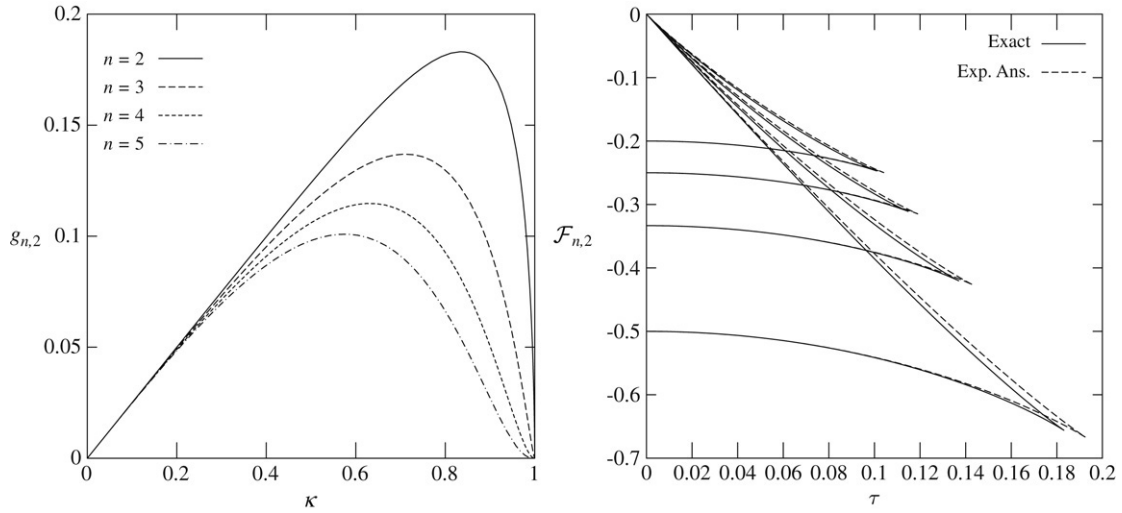

Fig. 5. Left panel: Functions $g_{n,2}(\kappa)$ for $n = 2, 3, 4, 5$. As n increases, the maximum of $g_{n,2}(\kappa)$ shifts towards $\kappa = 0$. Right panel: Comparison between the exact (Eq. (43)) and the approximate exponential ansatz (Eq. (49)) energies, $\mathcal{F}_{n,2}$ and $\tilde{\mathcal{F}}_{n,2}$, for $n = 2, 3, 4, 5$. The lowest curve corresponds to $n = 2$ and curves are shifted upwards as n increases.

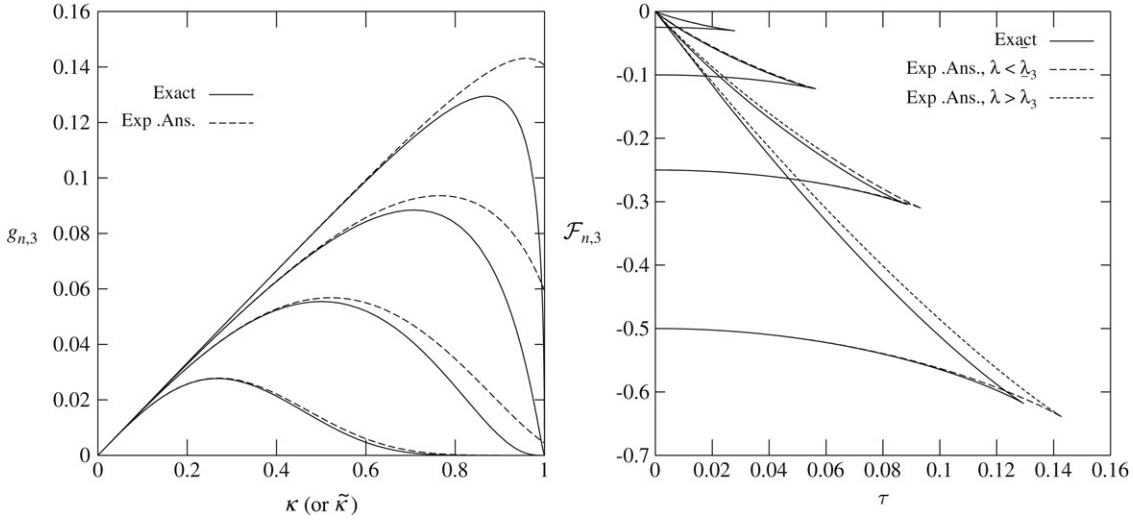

Fig. 6. Left panel: Functions $g_{n,3}(\kappa)$ for $n = 2, 4, 10, 40$ compared to their exponential ansatz counterparts $\tau(\tilde{\kappa})$ (see Eqs. (48) and (50)) evaluated with $\lambda \in [0, \bar{\lambda}_3]$, where $\bar{\lambda}_3 = 2 - \sqrt{3}$. Right panel: Comparison between the exact and the approximate exponential ansatz energies, $\mathcal{F}_{n,3}$ and $\tilde{\mathcal{F}}_{n,3}$, for the same values of n. The exponential ansatz solution is evaluated for $\lambda \in [0, \bar{\lambda}_3]$ (dashed line) and for $\lambda \in [\bar{\lambda}_3, 1]$ (dotted line).

4.3.3. Large nonlinearities, $n \to \infty$

We have seen in the previous section that evaluating the hopping threshold $\tau^*_{n,d}$ amounts to solving the equation $\mathrm{d}\tau/\mathrm{d}\kappa = 0$, that is $\mathrm{d}g_{n,d}(\kappa)/\mathrm{d}\kappa = 0$. Using the explicit expression (33), the latter translates into

$$(2n-1)\left(\mathcal{L}'_d(s)\right)^2 = (n-1)\mathcal{L}''_d(s)\mathcal{L}_d(s), \quad s = \frac{d}{\kappa}, \tag{44}$$

where the prime denotes a differentiation with respect to s. The key point is to observe that when n tends to infinity, a solution to (44) requires s to tend to infinity too. Then, using the expansion provided in (29), Eq. (44) becomes

$$\frac{1}{s^4} + \frac{d(4-n)}{s^6} + \frac{3d}{4}\frac{(6-10d)n + 23d - 11}{s^8} + \mathcal{O}\left(\frac{n}{s^{10}}\right) = 0 \tag{45}$$

which yields the asymptotic result $s^2 \sim nd + (7d-9)/2 + \mathcal{O}(n^{-1})$. Reinserting this value into (34) we find in leading order

$$\kappa^*_{n,d} \sim \sqrt{\frac{d}{n}}; \qquad \tau^*_{n,d} \sim \frac{\mathrm{e}^{-1/2}}{2\sqrt{nd}};$$
$$\mathcal{E}^*_{n,d} \sim -\mathrm{e}^{-1/2}; \quad \mathcal{F}^*_{n,d} \sim -\frac{2\mathrm{e}^{-1/2}}{n}, \qquad (n \to \infty). \tag{46}$$

Note that the evaluation of $\mathcal{F}^*_{n,d}$ requires the knowledge of the constant term in the expansion for s^2 (see above). That is why it is provided. To derive the other quantities, the leading term is sufficient. These asymptotic expressions are the generalization of those obtained in 1D in (41). A by-product of this asymptotic analysis is a proof, for hypercubic lattices of arbitrary dimensions, of a conjecture by Bustamante and

Molina [33] that the value of the Lagrange parameter $\mathcal{E}^*_{n,d}$ (bound state energy) of the SNI is universal. Indeed, in their paper, these authors have obtained strong numerical evidence that[8] $|\mathcal{E}^*_{n,d}| \sim 1/\sqrt{\mathrm{e}}$ as $n \to \infty$ for a wide variety of lattices. The result above shows that this is indeed the case for *hypercubic* lattices. But the same idea may be applied to Eq. (26) that is valid for an arbitrary lattice. Using a general asymptotic expansion of the lattice Green's function $G^{(0)}_{00}$, we show in Appendix E that the bound state energy $\mathcal{E}^*_{n,d}$ converges towards a universal value as the nonlinear exponent tends to infinity regardless of the detailed structure and the dimension of the lattice.

4.3.4. Approximate exponential ansatz solution to the SNI for $d > 1$

As we have seen previously, the exponential ansatz (EA) is the exact solution to the SNI in 1D. In higher dimensions, this is no longer the case. Nevertheless, the EA still proves to be a very useful approximate analytical solution, as we now establish. Using (10) and the energy $\mathcal{F}$ defined in (22) we find the following functional for the EA approach to the SNI problem:

$$\tilde{\mathcal{F}} = -\frac{1}{n}\left(\frac{1-\lambda^2}{1+\lambda^2}\right)^{nd} - \frac{4\tau d\lambda}{1+\lambda^2}. \tag{47}$$

The extrema of this functional are given by $\partial\tilde{\mathcal{F}}/\partial\lambda = 0$ which can immediately be solved for τ

$$\tau = \frac{\lambda}{1+\lambda^2}\left[\frac{1-\lambda^2}{1+\lambda^2}\right]^{nd-2}. \tag{48}$$

Reinserting this result into (47) and using (22), we obtain the energy and the Lagrange parameter as

$$\begin{aligned}\tilde{\mathcal{E}} &= -\left[\frac{1-\lambda^2}{1+\lambda^2}\right]^{nd}\left[1+\frac{4d\lambda^2}{(1-\lambda^2)^2}\right];\\ \tilde{\mathcal{F}} &= -\left[\frac{1-\lambda^2}{1+\lambda^2}\right]^{nd}\left[\frac{1}{n}+\frac{4d\lambda^2}{(1-\lambda^2)^2}\right]\end{aligned} \tag{49}$$

and we can also define $\tilde{\kappa} = -2d\tau/\tilde{\mathcal{E}}$, the EA approximation of the parameter κ, that reads

$$\tilde{\kappa} = \frac{2\lambda d(1+\lambda^2)}{(1-\lambda^2)^2+4d\lambda^2}. \tag{50}$$

Clearly, this expression is an approximate d-dimensional generalization of Eq. (36) that is recovered for $d = 1$. In 1D and 2D, $\tilde{\kappa}$ and λ are in one-to-one correspondence over the interval $[0, 1]$. But as soon as $d \geq 3$, this is no longer true and for $\lambda > \bar{\lambda}_d = d - 1 - \sqrt{(d-1)^2-1}$, the parameter $\tilde{\kappa}$ becomes larger than unity. This is the main drawback of the EA approach to the SNI problem, for the Lagrange parameter cannot penetrate into the continuum band. But the approximate expressions derived within the EA violate this condition unless the range of λ is restricted to $[0, \bar{\lambda}_d]$. Restricting the localization length parameter to such a range of values is not inconsequential, however. For instance, the resulting value of τ at $\lambda = \bar{\lambda}_d$ (i.e. $\tilde{\kappa} = 1$) is nonzero, which contradicts the prediction of the exact result in 3D and 4D. In 3D and 4D, the exponential ansatz creates a gap that does not exist for the unstable bound state (this is seen for $d = 3$ in Fig. 6, left panel). Nevertheless, in Fig. 6, we show that the energies $\tilde{\mathcal{F}}_{n,3}$ reproduce the exact ones well enough if we use the full range $\lambda \in [0, 1]$ in the parametric representation (49) and (48).This agreement must in some sense be regarded as accidental, given that the EA does not provide reliable results in the vicinity of the continuum band. From (48), we can calculate the critical localization length, $\lambda^*_{n,d}$, maximizing τ. It is given by

$$\lambda^*_{n,d} = \left[(2nd-3) - \sqrt{(2nd-3)^2-1}\right]^{1/2}. \tag{51}$$

It is easy to see that for $n \geq 2$ and $d \geq 3$, $\lambda^*_{n,d} < \bar{\lambda}_d$. This means that the value of the localization parameter at the maximum of τ is located within the portion of the graph where $\tilde{\kappa}$ is less than unity. This value is then admissible. Using (51), (48) and (49), we can evaluate all quantities at criticality and in particular, their asymptotic expression as $n \to \infty$

$$\begin{aligned}&\lambda^*_{n,d} \sim \frac{1}{2\sqrt{nd}}; \qquad \tilde{\kappa}^*_{n,d} \sim \sqrt{\frac{d}{n}}; \qquad \tilde{\tau}^*_{n,d} \sim \frac{\mathrm{e}^{-1/2}}{2\sqrt{nd}};\\ &\tilde{\mathcal{E}}^*_{n,d} \sim -\mathrm{e}^{-1/2}; \qquad \tilde{\mathcal{F}}^*_{n,d} \sim -\frac{2\mathrm{e}^{-1/2}}{n}.\end{aligned} \tag{52}$$

As we can see, these expressions are exactly the same as those derived from the exact SNI solution in (46). Hence, the approximate EA solution to the SNI problem becomes asymptotically correct at high nonlinearities. Moreover, Fig. 5 (right panel), which compares the energies of the exact and the EA solutions in 2D, shows that the accuracy of the latter is good even at low nonlinearities. The simple analytical expressions derived from this approximation are then useful to treat the SNI problem whose exact solution becomes dauntingly complicated as the dimensionality increases.

4.3.5. Exact localization parameter vs κ

As we have seen in the previous section, the EA does not provide a reliable relation between the localization parameter λ and the parameter κ. This is due to the angular dependence of the localization parameter. Indeed, in contrast to the EA whose wavefunction assumes a single localization parameter for all directions, $\tilde{\varphi}_{\boldsymbol{m}} \propto \lambda^{|\boldsymbol{m}|}$, the exact SNI wavefunction decays differently in different directions $\boldsymbol{m}$. We can define an *exact* direction-dependent localization parameter $\lambda_{\boldsymbol{m}}$ through

$$\begin{aligned}\ln\lambda_{\boldsymbol{m}} &= \lim_{\mu\to\infty}\frac{1}{\mu|\boldsymbol{m}|}\ln\left|\varphi_{\mu\boldsymbol{m}}\right|\\ &= \lim_{\mu\to\infty}\frac{1}{\mu|\boldsymbol{m}|}\ln\left|G^{(0)}_{\boldsymbol{0},\mu\boldsymbol{m}}(\mathcal{E})\right|,\end{aligned} \tag{53}$$

where we have used the fact that $|\varphi_{\boldsymbol{m}}|^2 = \mathrm{Res}_{z\to\mathcal{E}}G_{\boldsymbol{mm}}(z)$ together with Eq. (24). An asymptotic analysis done in

[8] To compare with [33], readers should note that in our case the nonlinear parameter γ is set to unity; it is easily reinserted using Eq. (9). Recall also that sign convention for the energy is opposite.

Appendix F shows that in the direction $\boldsymbol{m} = (1, \ldots, 1, 0, \ldots, 0)$, with m 1's and $d - m$ 0's, the leading order of the Green's function $G^{(0)}_{\mathbf{0},\mu\boldsymbol{m}}(\mathcal{E})$ reads

$$G^{(0)}_{\mathbf{0},\mu\boldsymbol{m}}(\mathcal{E}) \sim \frac{-1}{2\tau} \frac{\left[A_m - \sqrt{A_m^2 - 1}\right]^{\mu m}}{(2\pi\mu m)^{\frac{d-1}{2}}} \times m^{\frac{d}{2}-1} \frac{(A_m^2 - 1)^{\frac{d-3}{4}}}{A_m^{\frac{m-1}{2}}} \quad (\mu \to \infty), \tag{54}$$

where

$$A_m = \left(\frac{1}{\kappa} - 1\right)\frac{d}{m} + 1\,, \; m \in \{1, 2, \ldots, d\}. \tag{55}$$

Obviously, from Eqs. (53) and (54), the localization parameter can be expressed as

$$\lambda_{\boldsymbol{m}} = A_m - \sqrt{A_m^2 - 1}. \tag{56}$$

Inverting (56), we obtain κ as a function of $\lambda_{\boldsymbol{m}}$

$$\kappa = \frac{2d\lambda_{\boldsymbol{m}}}{m(1 - \lambda_{\boldsymbol{m}})^2 + 2d\lambda_{\boldsymbol{m}}}. \tag{57}$$

We see now that κ and $\lambda_{\boldsymbol{m}}$ are in one-to-one correspondence and that $\kappa = 0$ for $\lambda_{\boldsymbol{m}} = 0$ while $\kappa = 1$ when $\lambda_{\boldsymbol{m}} = 1$, which means that the wavefunction is not exponentially localized when the bound state energy reaches the continuum band-edge: it is at best algebraically decaying in this limit. The expression (57) is clearly different from the approximate EA solution given in Eq. (50) although the two formulae become equivalent in the limit of small λ (or small κ). Let us first notice that in 1D ($m = 1$ is the only possible value in this case), the expression (57) reduces to the formula already given in (36). Another interesting observation is that, in the $(1, \ldots, 1)$ direction ($m = d$), the expression (57) is equivalent to this 1D expression

$$\kappa \equiv \frac{-2\tau d}{\mathcal{E}} = \frac{2\lambda_{1,\ldots,1}}{1 + \lambda^2_{1,\ldots,1}}. \tag{58}$$

Thus, measuring the decay of the wavefunction in the $(1, \ldots, 1)$ direction is a simple way to obtain the bound state energy (Lagrange parameter) $\mathcal{E}$ of the SNI problem.

5. DNLS excitation thresholds

5.1. Exponential ansatz approach

The purpose of this final section is to determine excitation thresholds for the appearance of breathers in DNLS hypercubic lattices. Depending on the fixed parameters, any threshold will manifest itself as a minimum or maximum of a free quantity. It is convenient at this point to use the general form of the DNLS equation presented in Section 1.2 to follow one-parameter families of discrete breather solutions. Such families are typically obtained by tuning the amplitude of the breather while fixing two of the three quantities involved in Eq. (6) namely, the hopping $\hat{\tau}$, the nonlinear strength γ and the norm $\mathcal{N}$. The interdependence of these quantities is given by equation (8) that shows how they combine to form the effective hopping of a DNLS equation whose norm and nonlinear strength are set to unity. Once two parameters are fixed, the third one reaches an extremum at the threshold. For instance, if we fix the norm and the nonlinear strength, the hopping will be *maximum* at the threshold. Above this value, no breather exists. If the hopping and the norm are fixed, the nonlinear strength reaches a *minimum* at the threshold and so does the norm, if the hopping and the nonlinear strength are fixed instead.

In what follows, we focus on the families obtained by fixing the values of the hopping and the nonlinear strength while tuning the amplitude of the breather, ψ_0. The norm and the energy of the breather both turn out to be single-valued functions of the amplitude that can be reduced to arbitrary small values [22]. For large enough values of the amplitude, the breather is peaked around its center (site 0) and its norm is asymptotically given by $\mathcal{N} \sim |\psi_0|^2$ [23]. As the amplitude decreases, the breather broadens but if a threshold exists, the norm reaches a minimum $\mathcal{N}^*$ for some value of the amplitude ψ_0^* and increases again as the amplitude tends to zero. For $\psi_0 < \psi_0^*$ the breather is unstable while it is stable when $\psi_0 > \psi_0^*$ [20]. Numerical solutions to (6) with given amplitude are easily obtained with a version of the Proville–Aubry algorithm [34] modified to fix the amplitude of the breather rather than its norm. For convenience, we have set the hopping and nonlinear strength to unity. Monitoring the norm as a function of the amplitude, we obtain the curves of Fig. 7. As we can see, in 1D (upper-left panel), for $n = 2$ (cubic DNLS), the norm has no minimum and goes all the way down to zero as the amplitude decreases toward zero. This indicates the well-known fact that there is no threshold in the 1D cubic DNLS equation. In contrast, as long as $n \geq 3$, a threshold exists. In higher dimensions, Fig. 7 (upper-right and lower panels) shows that for $d \geq 2$ thresholds exist even for $n = 2$. In fact, according to Weinstein's result, thresholds exist in DNLS systems provided $d(n - 1) \geq 2$ [23]. We observe on these graphs that, regardless of the dimension of the lattice, the trend is that both ψ_0^* and $\mathcal{N}^*$ tend to 1 as the nonlinear exponent n increases. This means that the other components of the wavefunction ψ_j^*, $j \neq 0$, progressively vanish as $n \to \infty$. The increasingly important role of the central nonlinearity suggests an SNI solution to the DNLS problem in that limit.

Our goal is now to find a reliable explicit analytical approximation for the excitation threshold. As in the previous sections, we will once again make use of the exponential ansatz with the difference that its norm be now $\mathcal{N}$ rather than unity. Using

$$\tilde{\psi}_{\boldsymbol{m}} = \sqrt{\mathcal{N}}\left(\frac{1 - \lambda^2}{1 + \lambda^2}\right)^{d/2} \lambda^{|\boldsymbol{m}|}, \quad \lambda \in [0, 1], \tag{59}$$

and Eq. (7), we obtain the energy functional

$$\hat{\tilde{F}} = -\frac{\gamma\mathcal{N}^n}{n}\left[\left(\frac{1 - \lambda^2}{1 + \lambda^2}\right)^n \frac{1 + \lambda^{2n}}{1 - \lambda^{2n}}\right]^d - \frac{4\hat{\tau}\mathcal{N}\, d\,\lambda}{1 + \lambda^2}. \tag{60}$$

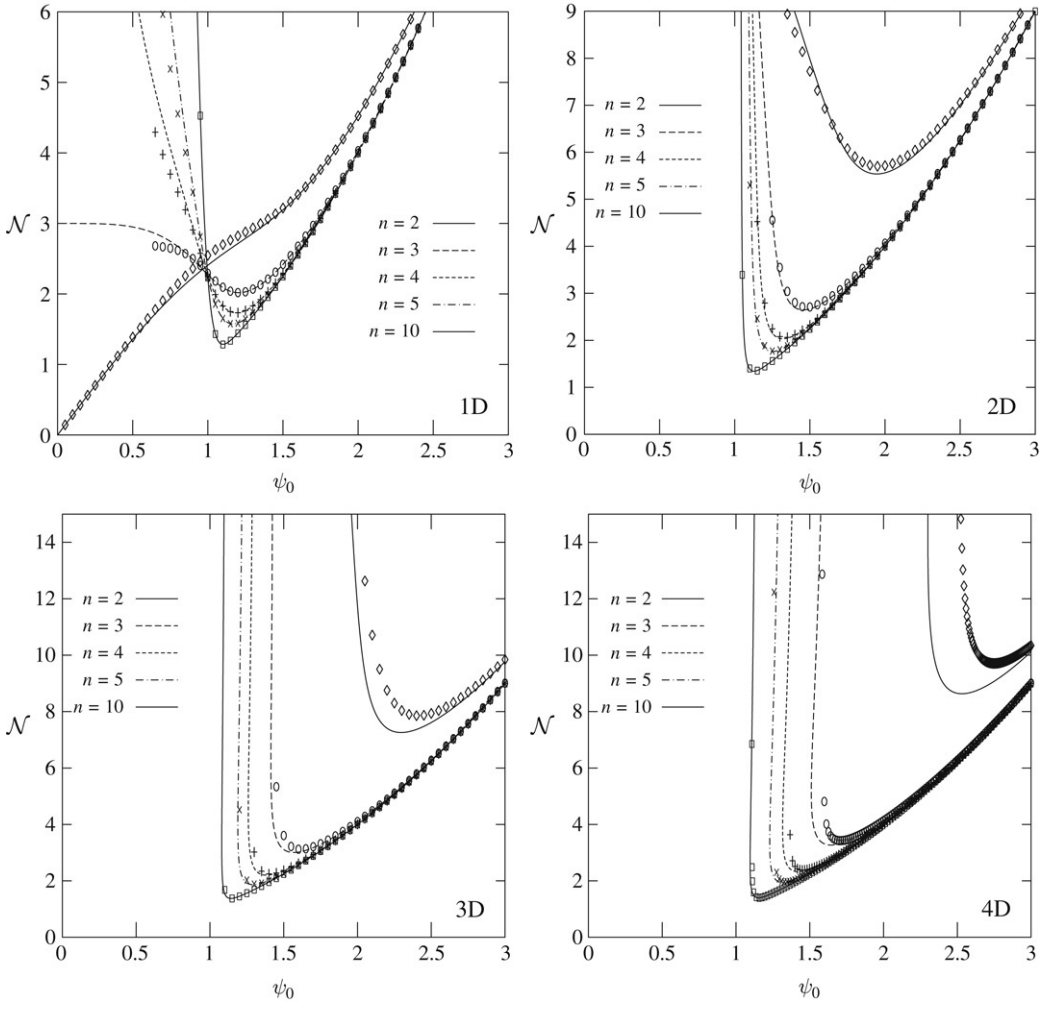

Fig. 7. Norm $\mathcal{N}$ vs amplitude ψ_0 in 1D, 2D, 3D, 4D for $n = 2, 3, 4, 5, 10$. The parameters $\hat{\tau}$ and γ are set to unity. Numerical results displayed as points are compared to the exponential ansatz result (lines) given in (62) and (61). The dimension of the lattice is indicated in the lower-right corner of the graph.

We can also directly obtain this result by using Eqs. (11), (8) and (9). Now, we find the extremum of $\hat{\tilde{F}}$ with respect to λ for a fixed norm[9] and solve for $\mathcal{N}$ to obtain

$$\mathcal{N}^{n-1} = -\frac{4\hat{\tau}}{\gamma(1+\lambda^2)^2}\frac{(1-\lambda^2)}{A_n(\lambda)^{d-1}A_n'(\lambda)}$$
$$\text{where } A_n(\lambda) = \left[\frac{1-\lambda^2}{1+\lambda^2}\right]^n \frac{1+\lambda^{2n}}{1-\lambda^{2n}}. \tag{61}$$

From Eq. (59), the amplitude is given by

$$\tilde{\psi}_{\mathbf{0}} = \sqrt{\mathcal{N}}\left(\frac{1-\lambda^2}{1+\lambda^2}\right)^{d/2}, \tag{62}$$

and we have thus obtained an approximate parametric representation for $\mathcal{N}(\tilde{\psi}_{\mathbf{0}})$, that is $(\tilde{\psi}_{\mathbf{0}}(\lambda), \mathcal{N}(\lambda))$, through the localization parameter $\lambda \in [0, 1]$. Similarly, by reinserting (61) into (60) we can obtain a parametric representation for the energy (or the Lagrange parameter) as a function of the amplitude. In Fig. 7, these approximate analytical solutions are compared to the numerical results. We see that they become quite accurate when the nonlinear exponent n increases. As a general trend, the EA solution becomes less accurate as the amplitude decreases, and this is particularly true after the threshold (minimum of the norm). Nevertheless, in most cases the threshold is well-reproduced by this approximation provided n is large enough. We also note that as the lattice dimension d increases the EA solution becomes less accurate for the lowest values of the nonlinear exponent n. Finally, despite the norms being single-valued functions of the amplitude, the approximate EA parametric expression, $(\tilde{\psi}_{\mathbf{0}}(\lambda), \mathcal{N}(\lambda))$, is not single-valued, as long as $d \geq 3$. This is because $\tilde{\psi}_{\mathbf{0}}(\lambda)$ is not monotonically decreasing as λ increases. It typically decreases up to some value λ' where it reaches a minimum, increases and decreases again towards zero as λ tends to 1. Nevertheless, the norm $\mathcal{N}(\lambda)$ reaches its minimum before λ', raising the possibility of capturing the threshold correctly.

[9] It is important to note that, although arbitrary, the norm is fixed. If not, the energy is unbounded.

Table 1
Numerical norm thresholds $\mathcal{N}^*_{n,d}$ in 1D, 2D, 3D and 4D for $\hat{\tau} = \gamma = 1$ and for various nonlinearities followed by the relative error of expression (63) with respect to the numerical result (in %)

n	1D		2D		3D		4D	
	$\mathcal{N}^*_{n,1}$	%	$\mathcal{N}^*_{n,2}$	%	$\mathcal{N}^*_{n,3}$	%	$\mathcal{N}^*_{n,4}$	%
2	–	–	5.7012519	8.8	7.8521534	11.0	9.7085587	13.4
3	2.0187163	0.92	2.7039808	2.23	3.1169024	3.60	3.4243891	4.55
4	1.7325176	0.02	2.0577604	1.20	2.2445921	1.88	2.3793423	2.31
5	1.5753225	5×10^{-4}	1.7742353	0.76	1.8874388	1.16	1.9681758	1.40
10	1.2858659	3×10^{-7}	1.3451997	0.18	1.3790034	0.27	1.4028796	0.31

5.2. Large n limit: SNI approach

We now turn to the determination of the excitation threshold. As we have seen, this corresponds to the minimum of the norm. Then, according to (61), it is obtained for the localization parameter $\lambda^*_{n,d}$ solution to $\partial\mathcal{N}/\partial\lambda = 0$. No exact analytical solution can be obtained for $\lambda^*_{n,d}$ for general d and n. Nevertheless, as n becomes large, we have seen previously that the central nonlinearity plays a dominant role and that the DNLS problem becomes asymptotically a SNI problem. This problem has already been treated in Section 4 for a wavefunction normalized to unity. Moreover, it has been demonstrated in Sections 4.3.3 and 4.3.4 that, when n becomes large, an exponential ansatz approach to the SNI problem leads to the same asymptotic results at the threshold. Then, using Eq. (8), we can estimate the norm threshold to be given by $[\mathcal{N}^*_{n,d}]^{n-1} \simeq \hat{\tau}/(\gamma\tau^*_{n,d})$ where $\tau^*_{n,d}$ is the EA approximation of the SNI effective hopping derived in (48) for the localization parameter $\lambda^*_{n,d} = [(2nd-3) - \sqrt{(2nd-3)^2-1}]^{1/2}$ given in (51). After some algebra, we find

$$\mathcal{N}^*_{n,d} \simeq \left[\frac{2\hat{\tau}}{\gamma}(nd-1)^{1/2}\left(\frac{nd-1}{nd-2}\right)^{\frac{nd}{2}-1}\right]^{\frac{1}{n-1}}, \quad nd > 2, \quad (63)$$

and from (62), the amplitude threshold reads

$$(\tilde{\psi}_0)^*_{n,d} \simeq \left[\frac{4\hat{\tau}^2}{\gamma^2}\frac{(nd-1)^{d-1}}{(nd-2)^{d-2}}\right]^{\frac{1}{4(n-1)}}, \quad nd > 2. \quad (64)$$

From Eqs. (63) and (64), we see that the norm and amplitude thresholds tend to unity as the nonlinear exponent n tends to infinity. This is confirmed by the numerical results. To assess the accuracy of the above expressions, we compare them to the numerical results in Table 1. The general trend is that, for a fixed dimension d, the expression (63) improves as n increases. But for a fixed nonlinear exponent n, the approximation deteriorates as d increases.

The approximate norm threshold (63) is seen to provide excellent results in 1D, but it is clearly poor for cubic nonlinearities ($n = 2$) in higher dimensions. Moreover, a striking difference exists between the 1D case and higher dimensions. Clearly, the expression (63) fails to improve as fast as in 1D when the nonlinearity increases. To understand whether this is due to the SNI approach itself or to its exponential ansatz solution, we have evaluated the SNI norm thresholds as follows: using the known analytical form for the Laplace transforms $\mathcal{L}_d(s)$ for $1 \leq d \leq 4$, we have calculated the functions $g_{n,d}(\kappa)$ defined in (33) and computed their maxima $\tau^*_{n,d}$. Then using Eq. (8) (with $\hat{\tau} = 1$ and $\gamma = 1$) we have evaluated the SNI norm thresholds as $\mathcal{N}^*_{n,d} = (\tau^*_{n,d})^{-1/(n-1)}$. As we have seen in Section 4.3.1, the EA solution to the SNI is exact in 1D. So the relative errors of the SNI thresholds with respect to the exact ones are the same as those provided in Table 1. They quickly improve as n becomes large. In higher dimensions results are quite similar. For $n = 2, 3, 4, 5, 10$, the following respective relative errors (in %) have been obtained for the exact SNI result. In 2D: 4.2, 0.07, 9×10^{-4}, 9×10^{-6}, $<10^{-7}$. In 3D: 1.6, 0.02, 10^{-4}, 10^{-6}, $<10^{-7}$. And in 4D: 0.82, 6×10^{-3}, 4×10^{-5}, $<10^{-7}$, $<10^{-7}$. Obviously, these results are quite different from those reported in Table 1. As in 1D, the relative errors decrease dramatically as n increases. Moreover, in contrast to the EA approximation to the SNI, they *improve as the dimension d increases*. Thus, the SNI approach to the threshold determination is accurate for virtually any n and d. Its main drawback, however, is that it requires the expression of the lattice Green's function in dimension d and even when the latter is known, its complexity generally precludes obtaining an analytical expression for the threshold.

Another approach to obtaining norm thresholds consists in using approximate Green's functions like those provided in Ref. [35] in 2D and 3D. For 3D lattices, the use of the so-called Hubbard Green's function yields[10] the approximate norm threshold $\mathcal{N}^*_{n,3} \simeq (3\sqrt{2n-1})^{1/(n-1)}(2n-1)/(2n-2)$ [46]. This expression gives a good result for $n = 2$ but fails to reproduce the correct asymptotic behavior (63) as $n \to \infty$. Moreover, for $n \geq 3$, the relative errors with respect to the exact threshold given in Table 1 are larger than that for the EA solution to the SNI. For $n = 2, 3, 4, 5, 10$ we find these relative errors (in %) to be 0.74, 3.87, 3.68, 3.24, 1.85, respectively. The lack of real improvement as n increases shows that a more accurate Green's function approximation is needed to catch the threshold correctly. In 2D dimensions, calculations based on the approximate Green's function provided in [35] are not amenable to a form simple enough to yield an explicit expression for the norm threshold [47].

[10] In Ref. [46], the threshold has been determined for $\gamma_{\text{Yiu}} \equiv \gamma/(6\hat{\tau}) = 1/(6\tau)$ (in our notation). The norm threshold is obtained by means of the relation $(\mathcal{N}^*)^{n-1} = 1/\tau^* = 6\gamma^*_{\text{Yiu}}$.

6. Summary and conclusions

We have studied nonlinear Schrödinger systems on hypercubic lattices in arbitrary dimensions. In the small hopping limit, $\tau \to 0$, we carried out a perturbative expansion of the onsite "discrete breather" wavefunction and evaluated its energy. For a nonlinear exponent n (see Eq. (4)), we show that the so-called *exponential ansatz* (EA) reproduced the exact results up to order τ^{4n-2} in 1D, whereas its accuracy is limited to order τ^2 in higher dimensions. The "excess" symmetry of the EA due to its factorized form was shown to be the reason why it loses its accuracy when $d > 1$. To improve this result, we analyzed a closely related system: a *single nonlinear impurity* (SNI) located at the center of an otherwise linear lattice. The reason for investigating such a problem is that, when approaching the anti-continuum limit ($\tau \to 0$), the breather wavefunction essentially localizes on one site, rendering the nonlinear contributions of the other sites negligible. The SNI solution is shown to match the exact solution up to order τ^{2n-2} in any dimension. More generally we prove that to achieve an accuracy of order τ^σ we need to keep the nonlinearities of the sites located in the hyperprism defined by the equation $2n|\boldsymbol{m}| \leq \sigma$, where $\boldsymbol{m} = (m_1, m_2, \ldots, m_d) \in \mathbb{Z}^d$ labels a particular site of the lattice and $|\boldsymbol{m}| = |m_1| + |m_2| + \cdots + |m_d|$. This result shows that in 1D, the EA is as accurate as the solution obtained by keeping the central (site 0) and nearest neighbor (site $+1$ and -1) nonlinearities.

We also analyzed the excitation thresholds for the existence of discrete breathers. These thresholds are known to appear as soon as the condition $(n-1)d \geq 2$ is met [23]. We first investigated the existence of such thresholds in the SNI problem. For a breather wavefunction normalized to unity, we derived an exact parametric expression for the total energy, the Lagrange parameter (also called bound state energy or frequency) and the hopping τ in terms of the Laplace transform of the dth power of the modified Bessel function I_0. The parameter $\kappa \in [0, 1]$ used to link these quantities is the ratio of half the bandwidth of the continuum to the bound state energy. It measures the "distance" of the bound state to the band edge of the continuum. With these expressions in hand we determined the excitation threshold as the maximum value of τ for which a breather exists. In 1D, we showed that the solution to the SNI problem is of the exponential ansatz type. We then linked the parameter κ with λ, the localization parameter of the exponential ansatz wavefunction. Within this approximation, we provided an exact analytical result for all quantities at the threshold as a function of n. In higher dimensions, for $2 \leq d \leq 4$, the existence of analytical expressions for the Laplace transforms involved in the parametric equations enabled us to study $\tau(\kappa)$. But the complexity of these transforms precluded any attempt to obtain an analytical expression for the threshold. Nonetheless, we were able to observe that, at the threshold, the parameter κ tends to zero as the nonlinear exponent n increases. Using this result and an exact expansion for the Laplace transform in this limit we finally obtained an asymptotic expression for all quantities at the threshold as $n \to \infty$. An important by-product of this analysis was that, using a similar technique, we proved a conjecture by Molina and Bustamante that the bound state energy tends towards a universal limit as n becomes large – in any dimension and for any lattice structure. We also studied the exponential ansatz solution to the SNI problem. Although approximate, the latter provides a useful analytical expression for the localization parameter that enables us to calculate the hopping and the various energies at the threshold. In particular, we showed that, as $n \to \infty$, the exact asymptotic solution of the SNI and its EA approximation are the same.

Finally, we used a rescaled version of the DNLS equation to study the existence and location of thresholds in the full nonlinear problem, without approximations. More specifically, all other parameters being fixed, we followed the norm of the discrete breather as a function of its amplitude and evaluated its threshold (minimum of the norm). We used an EA approach to obtain an approximate parametric representation for the norm as a function of the amplitude in terms of the localization parameter λ. The result proved to be excellent in 1D and good in higher dimensions, provided the nonlinearity n is large enough. We observed that, in any dimension, the norm and amplitude at the threshold tend to unity as $n \to \infty$, meaning that the discrete breather becomes localized on a single site. We then used the exponential ansatz to the SNI problem to obtain an approximate analytical formula for the amplitude and the norm at the threshold as a function of the hopping, the nonlinearity and the dimension. We found that, typically, this expression improves as n increases – and becomes asymptotically exact as $n \to \infty$ – but degrades as d becomes larger in contrast to the exact SNI solution that improves as both n and d increase. The last result suggests that the SNI threshold becomes asymptotically exact at high nonlinearity and also in high dimension.

Acknowledgments

The authors would like to express their gratitude to S. Flach and S. Aubry for the fruitful discussions on these topics.

Appendix A. τ-series for $\lambda_{n,d}$

$$\lambda_{2,d} = \tau + (4d-2)\,\tau^3 + (40d^2 - 42d + 10)\tau^5 + \left(\frac{1568}{3}d^3 - 840d^2 + \frac{1264}{3}d - 67\right)\tau^7 + o(\tau^7). \quad \text{(A.1)}$$

$$\lambda_{3,d} = \tau + (6d-3)\,\tau^3 + (90d^2 - 90d + 23)\tau^5 + (1764d^3 - 2646d^2 + 1344d - 232)\tau^7 + o(\tau^7). \quad \text{(A.2)}$$

$$\lambda_{4,d} = \tau + (8d-3)\,\tau^3 + (160d^2 - 120d + 22)\tau^5 + \left(\frac{12\,544}{3}d^3 - 4704d^2 + \frac{5216}{3}d - 210\right)\tau^7 + o(\tau^7). \quad \text{(A.3)}$$

For $n > 4$, we obtain the general expression

$$\lambda_{n,d} = \tau + (2\xi - 3)\,\tau^3 + (10\xi^2 - 30\xi + 22)\tau^5 + \left(\frac{196}{3}\xi^3 - 294\xi^2 + \frac{1304}{3}\xi - 211\right)\tau^7 + o(\tau^7), \quad \text{(A.4)}$$

where $\xi = nd$.

Appendix B. τ-series for the energies

B.1. Exponential ansatz result

$$\tilde{F}_{2,d} = -\frac{1}{2} - 2d\tau^2 - d\,(4d-3)\,\tau^4 - \frac{2}{3}d(40d^2 - 54d + 17)\tau^6 - \frac{d}{3}(784d^3 - 1512d^2 + 923d - 180)\tau^8 + o(\tau^8), \quad \text{(B.1)}$$

$$\tilde{F}_{3,d} = -\frac{1}{3} - 2d\tau^2 - 2d\,(3d-2)\,\tau^4 - 2d(30d^2 - 36d + 11)\tau^6 - 2d(441d^3 - 756d^2 + 438d - 86)\tau^8 + o(\tau^8), \quad \text{(B.2)}$$

$$\tilde{F}_{4,d} = -\frac{1}{4} - 2d\tau^2 - 4d\,(2d-1)\,\tau^4 - \frac{32d}{3}(10d^2 - 9d + 2)\tau^6 - \frac{\mathrm{d}}{6}(12\,544d^3 - 16\,128d^2 + 6848d - 957)\tau^8 + o(\tau^8). \quad \text{(B.3)}$$

B.2. Exact perturbative result

$$F_{2,d} = -\frac{1}{2} - 2d\tau^2 - d\,(6d-5)\,\tau^4 - 2d(32d^2 - 66d + 35)\tau^6 - d(1064d^3 - 3828d^2 + 4918d - 2147)\tau^8 + o(\tau^8), \quad \text{(B.4)}$$

$$F_{3,d} = -\frac{1}{3} - 2d\tau^2 - 2d\,(4d-3)\,\tau^4 - \frac{2d}{3}(164d^2 - 270d + 121)\tau^6 - 2d(1128d^3 - 1161 + 3130d - 3060d^2)\tau^8 + o(\tau^8), \quad \text{(B.5)}$$

$$F_{4,d} = -\frac{1}{4} - 2d\tau^2 - 2d\,(5d-3)\,\tau^4 - 8d(10 + 21d^2 - 27d)\tau^6 - \frac{d}{2}(14\,404d + 8408d^3 - 17\,424d^2 - 4619)\tau^8 + o(\tau^8). \quad \text{(B.6)}$$

Appendix C. Maple codes

The Maple codes that we have used to obtain the results of the previous appendix as well as Eqs. (12), (16) and (31) are accessible as "supplementary material" in the online version of this paper. There, we provide a PDF file, `AppendixC.pdf`, with a commented version of the codes. We also provide ready-to-use Maple worksheets containing the codes themselves. The codes calculating the exponential ansatz energy, $\tilde{F}_{n,d}$, and $\lambda_{n,d}$ for $n = 2, 3, 4$ and for $n > 4$ are named `ProgC11` and `ProgC12`, respectively. The codes evaluating the SNI energy, $\mathcal{F}_{n,d}$, and the exact perturbative energy, $F_{n,d}$, up to order τ^8 are called `ProgC2` and `ProgC3`, respectively. Typical use of these programs is as follows:

- Copy the program in a file named for example `file`.
- In the same directory, open Maple and type

```
> restart;
> read ''file'';
```

- For `ProgC3` only, enter the value of the dimension d ($d \geq 1$) and the nonlinear exponent n ($n \geq 2$) as required by the program.

Appendix D. Equations for $\varphi_{\{\boldsymbol{m}\}} \in \mathcal{S}$

We list hereafter the equations for the components $\varphi_{\{\boldsymbol{m}\}}$, $|\boldsymbol{m}| \leq 4$ which, together with (15), allow for the determination of the coefficients $\phi_j^{\{\boldsymbol{m}\}}$ in (13) and $\mathcal{E}_{2j}$ in (14).

$$-\tau\,\Delta\varphi_{\{\boldsymbol{m}\}} - |\varphi_{\{\boldsymbol{m}\}}|^{2(n-1)}\varphi_{\{\boldsymbol{m}\}} = \mathcal{E}\varphi_{\{\boldsymbol{m}\}} + o(\tau^{8-|\boldsymbol{m}|}). \quad \text{(D.1)}$$

Explicit expressions for the Laplacians read

$$\begin{aligned}
\Delta\varphi_{\{0\}} &= b_0\varphi_{\{1\}} + o(\tau^8)\\
\Delta\varphi_{\{1\}} &= \varphi_{\{0\}} + \varphi_{\{2\}} + b_1\varphi_{\{11\}} + o(\tau^7)\\
\Delta\varphi_{\{2\}} &= \varphi_{\{1\}} + \varphi_{\{3\}} + b_1\varphi_{\{21\}} + o(\tau^6)\\
\Delta\varphi_{\{11\}} &= 2\varphi_{\{1\}} + 2\varphi_{\{21\}} + b_2\varphi_{\{111\}} + o(\tau^6)\\
\Delta\varphi_{\{3\}} &= \varphi_{\{2\}} + \varphi_{\{4\}} + b_1\varphi_{\{31\}} + o(\tau^5)\\
\Delta\varphi_{\{21\}} &= \varphi_{\{31\}} + \varphi_{\{11\}} + \varphi_{\{22\}} + \varphi_{\{2\}} + b_2\varphi_{\{211\}} + o(\tau^5)\\
\Delta\varphi_{\{111\}} &= 3\varphi_{\{211\}} + 3\varphi_{\{11\}} + b_3\varphi_{\{1111\}} + o(\tau^5)\\
\Delta\varphi_{\{4\}} &= \varphi_{\{3\}} + o(\tau^4)\\
\Delta\varphi_{\{31\}} &= \varphi_{\{21\}} + \varphi_{\{3\}} + o(\tau^4)\\
\Delta\varphi_{\{22\}} &= 2\varphi_{\{21\}} + o(\tau^4)\\
\Delta\varphi_{\{211\}} &= \varphi_{\{111\}} + 2\varphi_{\{21\}} + o(\tau^4)\\
\Delta\varphi_{\{1111\}} &= 4\varphi_{\{111\}} + o(\tau^4),
\end{aligned}$$

where $b_k = 2(d-k)\theta(d-k)$ and $\theta(u) = 1$ if $u \geq 0$ and 0 else.

Appendix E. Bustamante–Molina conjecture

We show in this appendix that for an arbitrary lattice with a single nonlinear impurity of the type $|\psi_0|^{2(n-1)}\psi_0$, the energy $\mathcal{E}_n^*$ of the bound state obtained at the threshold value τ_n^* of the hopping converges towards a universal value as the nonlinear exponent n tends to infinity.

We start from a tight-binding Hamiltonian with hopping τ for an arbitrary lattice with normalized eigenstates $|\psi_\nu\rangle$ and energies $\tau\varepsilon_\nu$. Its lattice Green's function $G_{00}^{(0)}(\mathcal{E})$ is given by

$$G_{00}^{(0)}(\mathcal{E}) = \sum_\nu \frac{|\psi_{\nu,0}|^2}{\mathcal{E} - \tau\varepsilon_\nu}, \quad \text{(E.1)}$$

where the sum runs over all possible eigenstates and where $\psi_{\nu,0}$ denotes the value of the wavefunction at site 0. We introduce the quantity $k = \tau/\mathcal{E}$ and the function $H(k)$ such that $G^{(0)}_{00}(\mathcal{E}) = H(k)/\mathcal{E}$. Then

$$H(k) = \sum_\nu \frac{|\psi_{\nu,0}|^2}{1 - k\varepsilon_\nu} = \sum_{l=0}^{\infty} k^l \langle \varepsilon^l \rangle, \quad \text{where}$$
$$\langle \varepsilon^l \rangle = \sum_\nu |\psi_{\nu,0}|^2 \varepsilon_\nu^l. \tag{E.2}$$

As $\sum_\nu |\psi_\nu\rangle\langle\psi_\nu| = 1$, we have $\langle \varepsilon^0 \rangle = 1$. Moreover, without loss of generality we can fix the origin of the energies in the "middle" of the band, that is $\langle \varepsilon \rangle = 0$. Then, for k small enough, $H(k) \sim 1 + k^2\langle \varepsilon^2 \rangle + o(k^2)$.

Using the quantities defined above, Eq. (26) that provides the bound state energy $\mathcal{E}$ reads

$$\tau = -k \frac{[H(k)]^{2n-1}}{[H(k) + kH'(k)]^{n-1}}, \tag{E.3}$$

where the prime is a differentiation with respect to k. The maximum of τ yields the hopping threshold τ_n^*. Differentiating (E.3) with respect to k and equating to zero we finally obtain

$$H^2 + 2kHH' + (2n-1)k^2H'^2 - (n-1)k^2HH'' = 0, \tag{E.4}$$

where, for simplicity, the k-dependence of $H(k)$ has been omitted. Given the hypercubic lattice results, we safely anticipate that the solution k_n^* to (E.4) requires k to tend to zero as $n \to \infty$. With that in mind and the previous result that $H \sim 1 + k^2\langle \varepsilon^2 \rangle$, we see that the first term of Eq. (E.4) is of order 1, the next one of order k^2, the third one of order nk^4 and the last one of order nk^2. The second term is then negligible with respect to the first one and so is the third one with respect to the last. Hence, as $n \to \infty$, the first and last terms must cancel each other, which yields

$$(k_n^*)^2\langle \varepsilon^2 \rangle \sim \frac{1}{2n}. \tag{E.5}$$

Now, by definition, $\mathcal{E} = \tau/k$ and using both (E.3) and (E.5) we can evaluate the limit of the bound state energy $\mathcal{E}_n^* = \tau/k|_{k=k_n^*}$ as n tends to infinity. We find

$$\lim_{n\to\infty} \mathcal{E}_n^* = -\lim_{n\to\infty} \frac{[H(k)]^{2n-1}}{[H(k) + kH'(k)]^{n-1}}\bigg|_{k=k_n^*}$$
$$= -\lim_{n\to\infty} \frac{\left[1 + \frac{1}{2n}\right]^{2n-1}}{\left[1 + \frac{3}{2n}\right]^{n-1}} = -\frac{1}{\sqrt{\mathrm{e}}}. \tag{E.6}$$

This result establishes Bustamante and Molina's conjecture that the threshold bound state energy of the SNI problem converges to a universal value[11] as the nonlinearity of the impurity becomes infinite. The result above shows indeed that this limit does not depend on the detailed nature of the lattice as it does not depend on $\langle \varepsilon^2 \rangle$, the only lattice-dependent quantity involved in the calculation.

[11] See footnote 8.

Appendix F. Asymptotic analysis of $G^{(0)}_{\mathbf{0},n}(\mathcal{E})$ for some large $|\boldsymbol{n}|$

Here, we evaluate the asymptotic behavior of $G^{(0)}_{\mathbf{0},\mu\boldsymbol{n}}(\mathcal{E})$ when $\mu \to \infty$ where $\boldsymbol{n} = (n_1, n_2, \ldots, n_d)$ is a vector of integers indicating the direction towards which the decay of the Green's function is to be probed. Because of the hypercubic symmetry we can choose $n_1 \geq n_2 \geq \ldots, n_d \geq 0$ with $n_1 \geq 1$. Starting from its original expression

$$G^{(0)}_{\mathbf{0},\mu\boldsymbol{n}}(\mathcal{E}) = \frac{1}{(2\pi)^d} \int_{-\pi}^{\pi} \mathrm{d}^d k \frac{\mathrm{e}^{\mathrm{i}\boldsymbol{k}\cdot\boldsymbol{n}}}{\mathcal{E} + 2\tau \sum_{l=1}^{d} \cos k_l}, \tag{F.1}$$

we obtain after some manipulations

$$G^{(0)}_{\mathbf{0},\mu\boldsymbol{n}}(\mathcal{E}) = -\frac{\mu}{2\tau} \int_0^\infty \mathrm{d}z \mathrm{e}^{-\mu d\alpha z} \prod_{i=1}^{d} I_{\mu n_i}(\mu z), \tag{F.2}$$

where $\alpha = \kappa^{-1} = -\mathcal{E}/(2\tau d) \in [1, \infty]$ and where $I_m(z)$ is the modified Bessel function. Using the uniform asymptotic expansion of the latter provided in [37] we obtain

$$I_{\mu n_i}(\mu z) \sim \frac{1}{\sqrt{2\pi\mu}} \frac{\exp\left(\mu\left[\sqrt{n_i^2 + z^2} + n_i \ln \frac{z}{n_i + \sqrt{n_i^2 + z^2}}\right]\right)}{(n_i^2 + z^2)^{1/4}},$$
$$\mu \to \infty. \tag{F.3}$$

Reinserting this expression into (F.2), we see that

$$G^{(0)}_{\mathbf{0},\mu\boldsymbol{n}}(\mathcal{E}) \sim \lim_{\mu\to\infty} -\frac{\mu}{2\tau} \int_0^\infty \mathrm{d}z \mathrm{e}^{\mu f(\{n_i\};z)} g(\{n_i\}; z), \tag{F.4}$$

where

$$f(\{n_i\}; z) = \sum_{i=1}^{d} \left\{ \sqrt{n_i^2 + z^2} + n_i \ln \frac{z}{n_i + \sqrt{n_i^2 + z^2}} - \alpha z \right\}, \tag{F.5}$$

and

$$g(\{n_i\}; z) = \frac{1}{(2\pi\mu)^{d/2}} \prod_{i=1}^{d} \frac{1}{(n_i^2 + z^2)^{1/4}}. \tag{F.6}$$

We can prove that $f(\{n_i\}; z)$ has a single maximum at $z = z_0 > 0$. Differentiating $f(\{n_i\}; z)$ with respect to z, we obtain

$$f'(\{n_i\}; z_0) = 0 \Leftrightarrow \sum_{i=1}^{d} \sqrt{n_i^2 + z_0^2} = \alpha d z_0. \tag{F.7}$$

Let $h(z) = \sum_i \sqrt{n_i^2 + z^2} - \alpha d z$. Then $h'(z) = \sum_i z/\sqrt{n_i^2 + z^2} - \alpha d$ and $h''(z) = \sum_i n_i^2/(n_i^2 + z^2)^{3/2}$. Then, $h''(z) > 0$ for all z and $h'(z)$ is strictly increasing with z. But $\lim_{z\to\infty} h'(z) = d(1 - \alpha) < 0$, for $\alpha > 1$. Then, $h'(z) < 0$ and $h(z)$ is strictly decreasing as z increases. Now, $h(0) = \sum_i n_i > 0$ and $h(z) \sim (1 - \alpha)dz$ as $z \to \infty$ is surely negative in this limit. Consequently, there is a single solution

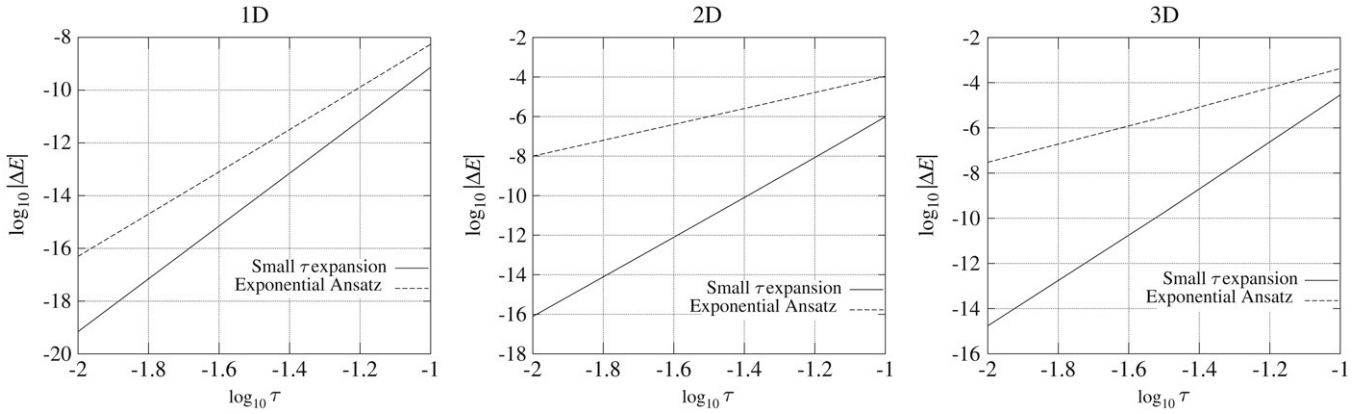

Fig. G.1. Energy differences, ΔE, between the numerical energy of a breather and its small τ expansion up to τ^8 (solid line) and its exponential ansatz approximation (dashed line) in $d = 1$ (left), $d = 2$ (middle), $d = 3$ (right) for $n = 2$. The linear dimension of the lattice is 21 sites.

$z_0 > 0$ to (F.7). Moreover, $f''(\{n_i\}; z) = -\sum_i n_i^2/z^2\sqrt{z^2+n_i^2}$ implies $f''(\{n_i\}; z_0) < 0$ □. Thus,

$$G^{(0)}_{\mathbf{0},\mu\boldsymbol{n}}(\mathcal{E}) \sim -\frac{\mu}{2\tau}\mathrm{e}^{\mu f(\{n_i\};z_0)}g(\{n_i\}; z_0)\sqrt{\frac{2\pi}{\mu|f''(\{n_i\}; z_0)|}}, \quad \mu \to \infty. \tag{F.8}$$

To proceed further, we need the solution to (F.7). For arbitrary parameters n_i an analytical solution is not known in general except in 2D, where it is easily obtained. We then solve the specific case where the m first n_i's are equal to 1 and the rest is equal to zero which means that we evaluate the asymptotic behavior of the Green's function in the direction $\boldsymbol{n} = (1, 1, \ldots, 1, 0, 0, \ldots, 0)$ with m 1's and $(d-m)$ 0's, $m \in \{1, 2, \ldots, d\}$. The solution to (F.7) is straightforward in this case and reads $z_0 = (A_m^2 - 1)^{-1/2}$ where $A_m = 1+(\alpha-1)d/m$ hence the result given in Eq. (54),

$$G^{(0)}_{\mathbf{0},\mu\boldsymbol{n}}(\mathcal{E}) \sim \frac{-1}{2\tau}\frac{\left[A_m - \sqrt{A_m^2-1}\right]^{\mu|\boldsymbol{n}|}}{(2\pi\mu|\boldsymbol{n}|)^{\frac{d-1}{2}}} \times m^{\frac{d}{2}-1}\frac{(A_m^2-1)^{\frac{d-3}{4}}}{A_m^{\frac{m-1}{2}}} (\mu \to \infty). \tag{F.9}$$

We have not been able to find this asymptotic expression, valid in arbitrary dimensions d, in the literature. Nevertheless, in some particular cases, it can be checked against some exact expressions for the Green's function. In 1D, Eq. (F.9) yields the result given by Economou in [35] (page 80, formula 5.28). In 2D, Katsura and Inawashiro provide an exact expression for the Green's function in terms of the hypergeometric function ${}_4F_3$ [43]. The latter is simplified in the (1, 1) direction to a ${}_2F_1$ function and using an asymptotic result given in Luke [44] (page 237, formula 11) we have been able to check the validity of (F.9). In the (1, 0) direction we have not been able to find any asymptotic result for the ${}_4F_3$ function in the literature but we have observed the validity of (F.9) numerically. In 3D, Joyce and Delves [45] provide an exact result in the (1, 1, 1) direction whose asymptotic behavior is reproduced by (F.9) too.

Notice that the leading order of the asymptotic expansion of $G^{(0)}_{\mathbf{0},\mu\boldsymbol{n}}(\mathcal{E})$ involves the l_1-distance $|\mu\boldsymbol{n}| = \mu m$ rather than the euclidean distance $\|\mu\boldsymbol{n}\| = \mu\sqrt{m}$. Nevertheless, when $\mathcal{E}$ comes close to the continuum band-edge, say $\mathcal{E} = -2\tau d + \delta\mathcal{E}$, we can expand Eq. (F.9) for $\delta\mathcal{E}$ small and we find

$$G^{(0)}_{\mathbf{0},\boldsymbol{n}}(\mathcal{E}) \sim \frac{-1}{2\tau}\left(\frac{|\delta\mathcal{E}|}{\tau}\right)^{\frac{d-3}{4}}\frac{\mathrm{e}^{-\|\boldsymbol{n}\|\sqrt{\frac{|\delta\mathcal{E}|}{\tau}}}}{(2\pi\|\boldsymbol{n}\|)^{\frac{d-1}{2}}} \quad (\|\boldsymbol{n}\| \to \infty, \delta\mathcal{E} \to 0). \tag{F.10}$$

In the 2D case, a similar expression[12] is given by Economou (see Eq. (5.46) of [35]). Thus, close to the continuum band-edge, a rotational invariance is recovered. This is due to the fact that the localization length becomes large in this limit and ignores the discreteness of the lattice, adopting finally the spherical symmetry of a punctual defect.[13] In the opposite limit, far away from the continuum, the distance involved in $G^{(0)}_{\mathbf{0},\boldsymbol{n}}$ is the l_1-distance appearing naturally in the small τ perturbation. In this case, the localization length is small and has a marked angular dependence induced by the hypercubic symmetry of the lattice.

Appendix G. Numerics

Fig. G.1 is a log–log $(\tau, \Delta E)$-plot showing the energy difference, ΔE, between the numerical energy of a single breather computed with the Proville–Aubry algorithm [34] and its small τ expansion up to τ^8 (solid line) in 1D, 2D and 3D for a cubic nonlinearity ($n = 2$). It shows also the energy difference between the exact energy and its exponential ansatz approximation (dashed line). The slope of the dashed line is 8 in 1D and 4 in 2D and 3D which shows that the exponential ansatz solution is accurate up to order τ^6 and τ^2, respectively. In contrast, it is 10 in all dimensions for the exact small τ expansion up to order τ^8, These results are in perfect agreement with those reported in Sections 2 and 3.

[12] A factor $(1/2V)$ is missing in this expression

[13] Although Eq. (F.10) has been obtained from a particular set of directions, it is general. Indeed, close to the continuum, $\alpha \sim 1$ and Eq. (F.7) leads to $z_0^2 \sim \sum n_i^2/(2d(\alpha-1))$. Reinstating this solution in (F.8), we obtain (F.10).

Appendix H. Supplementary data

Supplementary data associated with this article can be found, in the online version, at doi:10.1016/j.physd.2007.09.018.

References

[1] A.C. Scott, Nonlinear Science. Emergence and Dynamics of Coherent Structures, Oxford University Press Inc., New York, 2003.
[2] M.J. Ablowitz, B. Prinari, A.D. Trubatch, Discrete and Continuous Nonlinear Schrödinger Systems, in: London Mathematical Society Lecture Note Series, vol. 302, Cambridge University Press, 2004.
[3] Y.S. Kivshar, G.P. Agrawal, Optical Solitons: From Fibers to Photonic Crystals, Academic Press, London, UK, 2003.
[4] J.C. Eilbeck, P.S. Lombdahl, A.C. Scott, Physica D 16 (1985) 318.
[5] D.K. Campbell, S. Flach, Y.S. Kivshar, Phys. Today 57 (1) (2004) 43.
[6] T. Holstein, Ann. Phys. (N.Y.) 8 (1959) 325.
[7] A.S. Davydov, J. Theoret. Biol. 38 (3) (1973) 559.
[8] D.N. Christodoulides, R.I. Joseph, Opt. Lett. 13 (9) (1988) 794.
[9] A.A. Sukhorukov, Y.S. Kivshar, Phys. Rev. E 65 (2002) 036609.
[10] F.Kh. Abdullaev, et al., Phys. Rev. A 64 (2001) 043606.
[11] A. Trombettoni, A. Smerzi, Phys. Rev. Lett. 86 (2001) 2353.
[12] J.C. Eilbeck, M. Johansson, in: L. Vasquez, R.S. MacKay, M.P. Zorzano (Eds.), Localization and Energy Transfer in Nonlinear Systems, World Scientific, Singapore, 2003, p. 44.
[13] P.G. Kevrekidis, K.O. Rasmussen, A.R. Bishop, Internat. J. Modern Phys. B 15 (2001) 2833.
[14] Y.S. Kivshar, M. Peyrard, Phys. Rev. A 46 (6) (1992) 3198.
[15] Y.S. Kivshar, Phys. Lett. A 173 (2) (1993) 172.
[16] Y.S. Kivshar, M. Haelterman, A.P. Sheppard, Phys. Rev. E 50 (4) (1994) 3161.
[17] O. Bang, J.J. Rasmussen, P.L. Christiansen, Nonlinearity 7 (1994) 205.
[18] E.W. Laedke, K.H. Spatschek, S.K. Turitsyn, Phys. Rev. Lett. 73 (8) (1994) 1055.
[19] E.W. Laedke, O. Kluth, K.H. Spatschek, Phys. Rev. E 54 (4) (1996) 4299.
[20] B. Malomed, M.I. Weinstein, Phys. Lett. A 220 (1996) 91.
[21] M. Johansson, S. Aubry, Nonlinearity 10 (1997) 1151.
[22] S. Flach, K. Kladko, R.S. MacKay, Phys. Rev. Lett. 78 (7) (1997) 1207.
[23] M.I. Weinstein, Nonlinearity 12 (1999) 673.
[24] M. Kastner, Phys. Rev. Lett. 92 (10) (2004) 104301.
[25] P.G. Kevrekidis, K.O. Rasmussen, A.R. Bishop, Phys. Rev. E 61 (4) (2000) 4652.
[26] M. Johansson, K.O. Rasmussen, Phys. Rev. E 70 (2004) 066610.
[27] J. Dorignac, S. Flach, Physica D 204 (2005) 83.
[28] G. Kalosakas, S. Aubry, G.P. Tsironis, Phys. Rev. B 58 (6) (1998) 3094.
[29] P.G. Kevrekidis, et al., Phys. Rev. E 72 (2005) 046613.
[30] J. Dorignac, J. Zhou, D.K. Campbell, Physica D 216 (2005) 207.
[31] M.I. Molina, G.P. Tsironis, Phys. Rev. B 47 (22) (1993) 15330.
[32] M.I. Molina, Phys. Rev. B 60 (4) (1999) 2276.
[33] C.A. Bustamante, M.I. Molina, Phys. Rev. B 62 (23) (2000) 15287.
[34] L. Proville, S. Aubry, Eur. Phys. J. B 11 (1999) 41.
[35] E.N. Economou, Green's Functions in Quantum Physics, Springer-Verlag, 1983 (Chapter 6).
[36] G.S. Joyce, J. Phys. A 36 (2003) 911.
[37] M. Abramowitz, I.A. Stegun, Handbook of Mathematical Functions, Dover publications, Inc., New York, 1972 (Chapter 9.6–9.7).
[38] Maple 10. Maplesoft, a division of Waterloo Maple, Inc., 2006.
[39] A.P. Prudnikov, Yu.A. Brychkov, O.I. Marichev, Integrals and Series, vol. 4, Gordon and Breach Science Publishers, 1992, 1 p. 313, 3 p. 341, 35 p. 346.
[40] M.L. Glasser, E. Montaldi, Phys. Rev. E 48 (4) (1993) R2339.
[41] G.S. Joyce, J. Phys. A 31 (1998) 5105.
[42] M.L. Glasser, A.J. Guttmann, J. Phys. A 27 (1994) 7011.
[43] S. Katsura, S. Inawashiro, J. Math. Phys. 12 (8) (1971) 1622.
[44] Y.L. Luke, The Special Functions and their Approximations, vol. 1, Academic Press, New York, 1969.
[45] G.S. Joyce, R.T. Delves, J. Phys. A 37 (2004) 3645.
[46] Y.Y. Yiu, K.M. Ng, P.M. Hui, Phys. Lett. A 200 (1995) 325.
[47] K.M. Ng, Y.Y. Yiu, P.M. Hui, Solid State Commun. 95 (1995) 801.